Programming Sequential Reagent Delivery Using a

Pseudo – One Dimensional Paper Network

Shivani Dharmaraja

A thesis submitted in partial fulfillment of

the requirements for the degree of

Master of Science in Bioengineering

University of Washington

2013

Committee:

Barry Lutz

Wendy Thomas

Program Authorized to Offer Degree: Bioengineering

University of Washington

ABSTRACT

Programming Sequential Reagent Delivery Using a Pseudo – One Dimensional Paper Network

Shivani Dharmaraja

Chair of the Supervisory Committee:
Barry Lutz, Research Assistant Professor
Department of Bioengineering

Lateral flow tests (LFTs) have been identified as a diagnostic technology well suited for point-

of-care use in low resource settings. In addition to being rapid, affordable, disposable, and easy to

use, fluid transport of sample and reagents through the device occurs due to the capillary pressure

of the strip material, rather than through the use of pumps. While strip based LFTs are generally

limited to performing a single fluidic step, LFTs can be reconfigured into two-dimensional paper

networks (2DPNs) that automatically carry out multi-step fluidic operations. Development of a

functional 2DPN, however, is largely based on an "estimate and check" method – a process that

may require multiple iterations before achieving an appropriate device design.

Here, we use simple electrical circuit analogies of capillary pressure, fluidic resistance, and

volumetric flow rate to model the fluidic behavior of 2DPN devices and predict designs with the

desired functionality. We identify key design principles for a previously-developed 2DPN and

introduce an alternative linear network (Psuedo-1DPN) that is similar in appearance to the classic strip LFT, but can perform the discrete sequential fluid delivery required of a multi-step assay. Tuning the capillary pressure and geometry of the device, we can predict the experimentally observable release trends of multiple assay reagents. Furthermore, this model allows the ability to easily modify design parameters, such as reagent volume, spacing between delivery steps, and total number of delivery steps, such that the desired system behavior is achieved. Additionally, we quantitatively characterize the impact fluid source pad materials have on the reagent release through a strip, a critical tool for both identifying appropriate fabrication materials and predicting overall system behavior. We find that materials of different porosity and structure exhibit unique fluid release profiles; both the delivery rate and total percentage of fluidic content released over time will dramatically vary given the type of material used in device. Finally, we use these design capabilities to demonstrate the utility of this Pseudo-1DPN using a multi-step, enzyme-linked immunosorbent (ELISA) based assay for human immunodeficiency virus (HIV) p24 antigen.

TABLE OF CONTENTS

TABLE OF FIGURES

ACKNOWLEDGEMENTS

Chapter 1: Introduction

1.1 Motivations

Point-of-care (POC) diagnostics are tools specifically designed to be utilized at or near the site of patient care [1]. POC diagnostics have gained significant support and recognition for their ability to provide rapid results and allow for earlier treatment intervention, improved clinical outcome, and a more streamlined healthcare process [2]. In 2006, the total global POC testing market was estimated to be ten billion dollars, accounting for approximately 36% of the entire global diagnostic testing market [3]. Furthermore, this market is estimated to drastically grow over time, with the market for POC diagnostics expected to increase to 16.5 billion dollars by 2016 and 34.6 billion dollars by 2021 [4].

Utilization of POC diagnostics allows the opportunity for improved healthcare in both the developed and developing worlds [5]. In the developed world, requirements of a diagnostic tool largely depend on the acceptable result turnaround time, ease of specimen handling, and test complexity [5]. Result turnaround time is not critical and the specimen can stably be transported (in a timely manner) a reference laboratory, where specialized testing can be conducted using complex, high throughput instrumentation [5]. In contrast, at a physician's office, if the diagnostic method for the target of interest is both "simple" and has an "insignificant risk of an erroneous result" (as stated by the Food and Drug Administration (FDA)), POC diagnostics can be performed at a physician's office to provide rapid patient results during the course of single

visit. Similarly, POC tests can be of great value to home users, emergency responders, and the military. Individuals can anonymously self-screen themselves for potentially sensitive infections, such as human immunodeficiency virus (HIV) and sexually transmitted infections (STIs), in a limited medical resource setting [6,7]. Emergency responders and the military can utilize POC tests to quickly detect exposure to specific biothreat agents that may have been released, as well as diagnose common illnesses and infections found the field [8].

POC diagnostics offer an even greater potential for improving healthcare systems in the developing world. Overall, public health has substantially progressed over the past few decades; however, because many of the benefits and services taken for granted in the developed world are lacking in the developing world, this progress has been dramatically unequal between the two sectors (**Figure 1**) [8,9]. Approximately 50% of the world's population lack basic sanitation, 20% do not have reliable electricity, and over 15% do not have basic healthcare services or clean drinking water [8,10]. While less than 5% of deaths in the world's richest countries are attributed to infectious diseases, more than 50% of deaths in the poorest countries result from the same causes [11,12].

Diagnostic tools used by the developed world are generally unsuitable for use in low resource settings due to an insufficient infrastructure (*i.e.*, limited capital, electricity, and skilled personnel) [13]. As a result, clinical treatment is generally initiated based on a patient symptoms and the local prevalence of particular diseases. While this syndromic management has been found to be effective and cost-efficient for cases of diseases that exhibit clear symptoms, it can

lead to unnecessary and/or incorrect treatment plans and acceleration of drug resistance in a given population [14]. In addition, asymptomatic patients infected with an illness may remain unaware of their status, potentially leading to worse patient outcome and increased transmission throughout the population. Implementation of a POC device appropriate for these settings has the potential to drastically reduce disease incidence over time and improve health outcomes throughout a population.
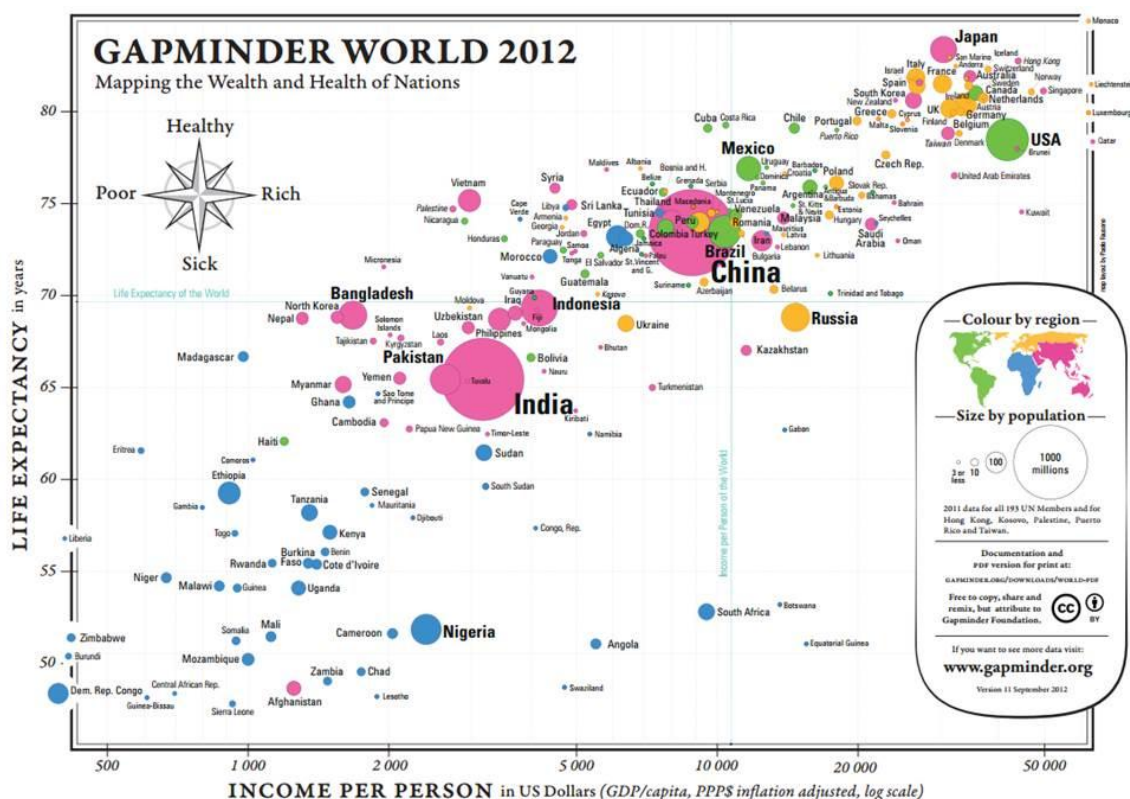
Figure 1. Correlation between income of a country and its population's average life expectancy [figure source: *free material from www.gapminder.org]. On average, life expectancy (in years) increases with country income (per person). The America's and Europe generally show an average life expectancy of greater than 70 years. To contrast, the life expectancy in a large number of African countries ranges from less than 50 years to approximately 65 years.*

1.2 Requirements of a Point-of-Care Diagnostic

Healthcare facilities in low resource settings often have a very low budget, limited or unreliable electricity, and few and/or untrained personnel. To match these constraints, the World Health Organization (WHO) Sexually Transmitted Disease Diagnostics Initiative developed general guidelines for the development of a POC diagnostic test that is relevant in the developing world [15,16]. This well-accepted ASSURED criteria states that diagnostics should be: Affordable, Sensitive, Specific, User-friendly, Rapid and robust, Equipment-free, and Deliverable [17].

Devices should be of a price that is appropriate to their target audience, while still maintaining an acceptable sensitivity and specificity level. Low specificity and sensitivity can cause unreliable test results and lead to health workers distrusting, or completely ignoring, patient diagnoses. Additionally, the training level of healthcare workers in the developing world can dramatically vary, with test users often being community health care workers with little scientific background [5]. To accommodate this and ensure that tests are being correctly performed, diagnostics must be user-friendly, with minimal complexity.

Another critical feature of a POC device is that it must be rapid. It is common for patients to travel great distances before reaching a healthcare center. If the patient is forced to make multiple visits to the center before receiving their diagnosis and starting treatment (similar to what occurs in the developed world), it is likely that a significant percentage of patients will be lost to follow-up and go untreated and unaware of their health status. A study performed in Thailand showed that approximately 41% of women found to have abnormal pap smears were

lost to follow-up [18]. They attributed this high magnitude of loss to patients: 1) not being properly notified of their test results, 2) not understanding their informed letter, 3) not realizing the seriousness of their medical results, and 4) having travel-related issues [18]. However, if the diagnostic tool is rapid, patients can theoretically have an initial consultation, be diagnosed, and start treatment all within the same visit, minimizing the likelihood of these complications.

Relevant POC diagnostics should also function without the use of any equipment. This is both to meet the common limitations of laboratory infrastructure in low resource settings and ensure that the quality of the diagnostic's results is not negatively impacted by faulty equipment. Equipment that requires use of electricity may not be well utilized, as power sources in many clinical settings may be either unavailable or unreliable. Additionally, without proper quality control methods, substandard, broken, or improperly calibrated equipment can easily go undetected, and introduce errors in the diagnostic's output. POC diagnostics should be entirely self-contained.

Finally, POC diagnostics should be easily deliverable to regions in need. This means that the devices should be stable at a wide variety of temperatures for a significant period of time.

The requirements for a POC diagnostic test to be relevant in LRS are extensive. However, a device that is able to fulfill these criteria has the potential to have a significant impact on healthcare in the developing world.

1.3 Current Point-of-Care Diagnostic Technologies

Existing technologies used for POC testing include imaging, flow cytometry, microfluidics, and immunoassays [5]. Optical imaging is currently one of the most trusted methods of malaria and TB diagnosis. High-magnification transmission light microscopy is used to identify the number of malarial parasites in a patient's stained blood smear sample, and fluorescence microscopy is used to detect TB [19,20]. Strides in technology have allowed for optical microscopes and digital cameras to be reasonably priced for purchase in some LRS (~$500) [5]. However, preparation of patient samples generally requires trained personnel and without specialized automated image analysis software, image capture and analysis can be a time-consuming process, making it difficult for laboratories to maintain the large number of patients commonly observed in afflicted regions [5,21].

Flow cytometry allows the ability to count cells based on their morphology or their expression of specific surface antigens in a high throughput manner. Some applications have included staging HIV progress, detecting the presence of cancerous cells, and diagnosing and monitoring immune dysfunction [22–26]. However, this technology can be expensive and is generally unreasonable for LRS. Over the past few years, there have been efforts to use microfluidics technology to reduce the cost and complexity of flow cytometry instruments [27]. Unfortunately, commercialization of these devices has had limited success [5].

Microfluidic-based technologies consist of micron-sized channels used to manipulate small fluid volumes. Devices have been shown to have a wide range of medical diagnostic capabilities.

Microfluidic devices have been used to perform applications that include sample preparation, purification, and cell sorting [28–31]. However, the need for permanent instrumentation to operate these devices and retrieve quantitative results causes these technologies to be relatively high in cost (**Figure 2A,B**). Converting microfluidics systems into entirely disposable devices allows their cost to be drastically reduced, making them a system that may be relevant for many LRS [32].

Laboratory immunoassays are another commonly used diagnostic technique in LRS. An example of such an assay is an enzyme-linked immunosorbent assays (ELISA), which allows for highly sensitive and quantitative analyte detection, while still being low in cost. Briefly, a capture antibody that is specific to the detection analyte of interest is incubated on the bottom of a well
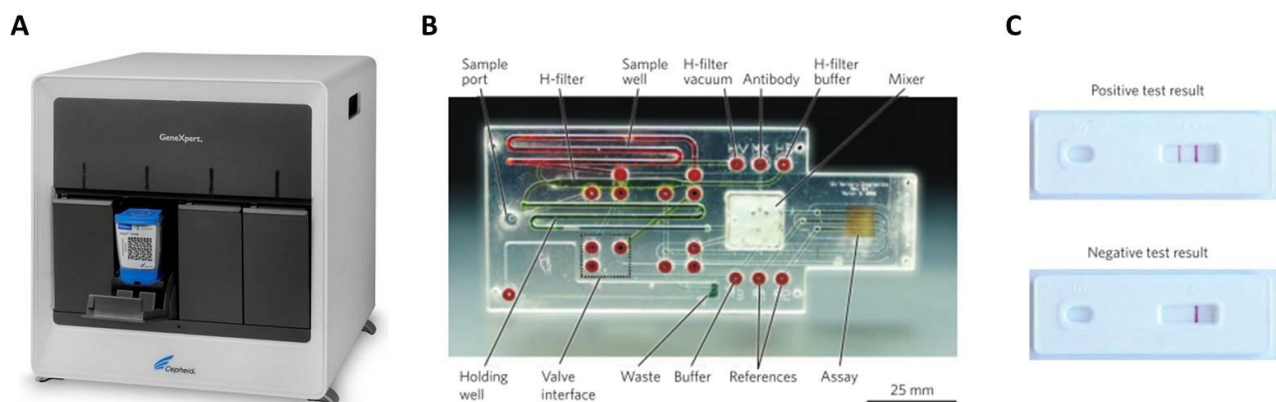
Figure 2. Examples of current POC diagnostic technologies. A) The GeneXpert (commercialized by Cepheid) is a disposable cartridge-based, automated diagnostic test that can identify Mycobacterium tuberculosis and resistance to rifampicin. The system is highly sensitive and rapid but too expensive for most LRS (~$17,000 for the system and ~$10 per cartridge). B) An image of a disposable microfluidics- based diagnostic card. External components are required for fluid control and movement (i.e., pumps, valves). C) Lateral flow strip test for gonorrhea. Sample is introduced to the membrane and a biochemical reaction occurs, presenting a visually observable result. [figure sources: a) axonlabs.com, b,c) Yager, et al., "Microfluidics diagnostic technologies for global public health," Nature 442 (2006) 412-18]

(from a well plate). All remaining surfaces of the well are blocked to reduce non-specific analyte adsorption and the well is subsequently incubated with the sample of interest, allowing analyte to bind to the capture molecule. Unbound analyte is washed away and a labeled marker specific to the analyte is introduced to bind captured analyte. An enzyme-linked reaction is then used to amplify the signal produced by the labeled marker. Additional forms of immunoassays have included optical, electrical, and mechanical elements as well [33–35]. However, many of these immunoassays (including ELISAs) are very time consuming to perform and require trained personnel, stringent reagent storage conditions, and external equipment to provide quantitative signal readout. A popular variation of these conventional immunoassays is the lateral-flow strip test, which is a rapid, paper-based immunoassay test (**Figure 2C**). Commonly used in the developing world, these tests are inexpensive, easy to use, and easy to store. We further discuss the advantages and disadvantages of this diagnostic system in the following section.

1.4 Paper-Based Microfluidics

Paper-based lateral flow strip tests have been identified as a diagnostic technology well suited for POC use in low resource settings [8,36]. With fluid transport occurring due to the capillary pressure of the porous strip material (rather than through the use of pumps), lateral flow strip tests are entirely disposable, rapid, user-friendly, and affordable [37–39]. The basic function of a lateral flow device is to mix sample with a visible label (*e.g.*, antibody conjugated to gold nanoparticles) and capture the analyte-label complex at a detection line via an immobilized capture molecule (*e.g.*, antibody) (**Figure 3**). A yes/no diagnosis can then be determined based
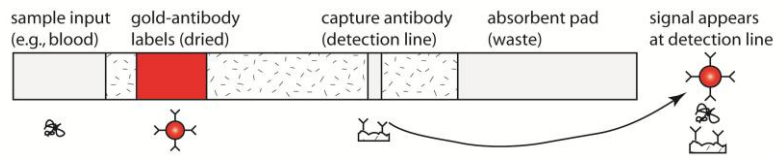
Figure 3. A common format for lateral flow tests. Fluid movement is driven by wicking, and chemical reagents are stored on the device. Most LFTs perform single-step sandwich immunoassays by binding a label to the analyte, then capturing the analyte-label complex at a detection line. In a LFT, these two reactions are carried out in a single fluidic step. LFTs typically cannot perform chemistries that require multiple steps (e.g., amplification, sample preparation).

on the presence of a visual signal produced by this binding event. Numerous lateral flow strip tests have already been developed and successfully used in low resource settings, with applications including pregnancy testing and disease diagnosis. While the simplicity of these strip tests makes them an ideal POC tool, it has generally limited them to performing tests that can be carried out in only a single fluidic step. Furthermore, using lateral flow tests (LFTs) as clinically relevant diagnostic tools is sometimes limited to targets with high(er) concentrations because of the limited analytical sensitivity of the LFT format. Recently, many research groups have been rethinking the advantages and limitations of LFTs and creating new devices with similar simplicity but added features, such as multiple assays contained within a single device [36,38,40–45].

In recent years, the Fu/Lutz/Yager group at UW has worked to increase the functionality of LFTs by patterning the membrane into two-dimensional paper networks (2DPNs) [46–53]. Utilizing non-linear geometries of a wicking membrane makes it possible to perform automated multi-step assays without greatly increasing the device complexity from a user-standpoint. **Figure 4** shows an early demonstration of a 2DPN designed to deliver three fluids to a detection

zone in a timed sequence. The three-legged device was contacted with three fluid droplets to initiate flow. The fluids initially wicked into the strip and met at the midway point between legs, followed by wicking of the fluids toward the detection region on the right of the strip (**Figure 4A,B**). Delivery from each leg stopped when its source fluid became depleted. The result was treatment of the detection zone with three fluids in a timed sequence (**Figure 4C**).

Sequential delivery in 2DPNs is controlled by two principles: 1) arrival time of each fluid at a detection zone is controlled by the length of the path followed by that fluid, and 2) fluid sources of finite volume are "shut off" once they are depleted. Thus, 2DPNs represent a form of fluidic programming that depends on wicking properties of the materials and the system-level behavior of paper networks.
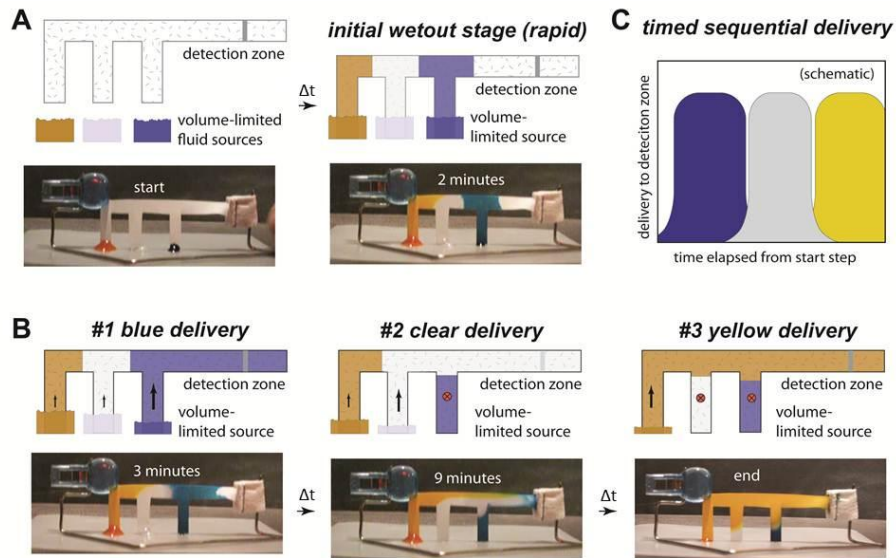
Figure 4. Early concept and demonstration of a 2-dimensional paper network (2DPN) for automated sequential fluid delivery. The device was fabricated from a porous nylon membrane cut by scissors, an absorbent pad (paper towel stapled to the membrane), and support stand (bent paper clip). Three drops of source fluid (water with food coloring) were pipetted onto a table, and flow was initiated by contacting the legs with droplets. Imperfections in sequential delivery (parallel flows of yellow and colorless fluids) can be seen in the images. The width of the main channel in the device was approximately 6 mm, and total time was about 9 minutes.

Since the initial concept demonstration (*circa* 2008), the Fu/Lutz/Yager group has developed devices that automatically perform multi-step immunoassays using enzyme-based signal amplification (ELISA chemistry) and electroless gold deposition onto gold detection labels for signal enhanceme nt [53–55]. Design variations have included card-like formats that used porous pads as fluid sources and a cartridge format that used a single fluid well as the source for all legs (**Figure 5**) [51,53–55]. **Figure 5** shows a previous example of a 2DPN that used porous (glass fiber) pads as the fluid sources [54]. The image sequences at left show delivery of colored fluids, and those at right show the same device performing a multi-step signal enhancement. Glass fiber pads were chosen because they release nearly all fluid, but as we later find, what
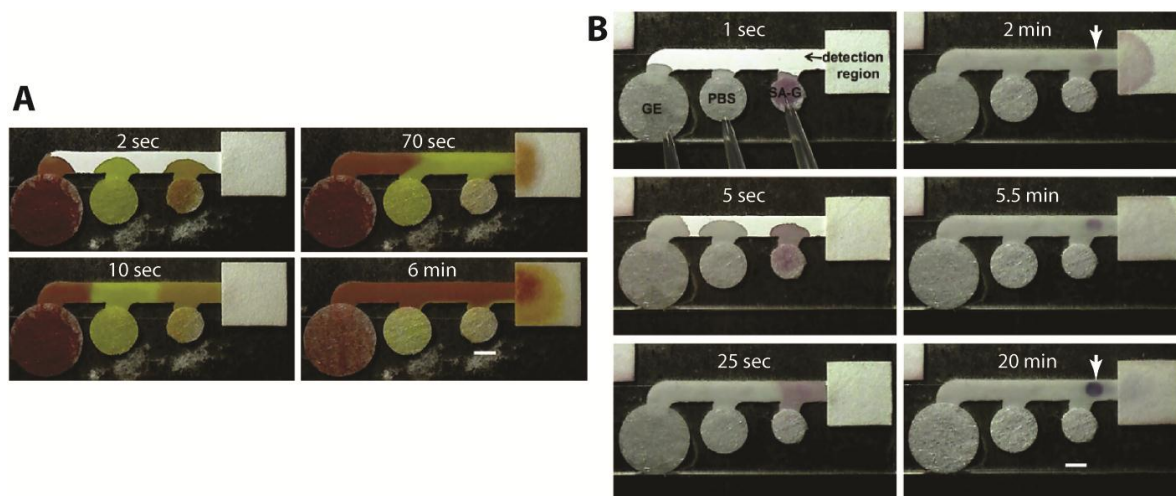
Figure 5. A 2DPN designed to automate a multi-step signal amplification [figure source: Fu, Kauffman, Lutz, Yager, "Chemical signal amplification in two-dimensional paper networks," Sensors & Actuators B 149 (2010) 325–328]. Porous (glass fiber) pads were used to hold finite volumes of source fluids. A) Image sequence of delivery of three fluids to a common leg in a timed sequence (orange, yellow, red). B) Image sequence for a sandwich immunoassay using a multi-step signal amplification process (SA-G: streptavidin-gold; PBS: phosphate-buffered saline; GE: gold enhancement reagent). The upper right image shows a faint gold spot (end point of a typical LFT), and the lower right image shows the darkened spot after enhancement. The device carried out all delivery steps without intervention. The width of the main channel was 3 mm.

appeared to be an ideal source actually is not. Successful fluidic sequencing depends not only on the paper network design but also on the release properties of the fluid sources.

When we compare the potential of these 2DPN devices to both ELISA and conventional strip LFT diagnostic tools, in the context of the ASSURED criteria, we see the utility that they might have in the field of diagnostics (**Table 1**). ELISA tests are highly sensitivity and specific, making them a very reliable diagnostic assay; however, their complicated and time consuming protocol, and equipment requirements do not make them well-suited for the POC. Conventional LFTs offer a drastically improved platform for a POC device – they are affordable, rapid, easy to use, and require no additional equipment. The analytical sensitivity and specificity of these devices, however, is often limited due to their ability to perform only one chemical reaction. The multi-step nature of a 2DPN offers an opportunity to improve upon the sensitivity and specificity of a conventional LFT [53–55]. In principle, enzyme-linked signal enhancement chemistries can potentially be used to improve the analytical sensitivity limits of a device and the inclusion of wash steps between reagent delivery steps may be useful in improving device specificity.

One difficulty of developing a functional 2DPNs is that they are generally designed using an "estimate and check" method. This method is effective but generally requires multiple iterations to achieve sequential delivery with minimal overlap in the delivery of fluids. Our goal is efficient, rational design of 2DPN devices. This requires an understanding of the physical properties, namely the capillary pressure and the fluid resistances, of the multiple materials within the paper network.

Table 1. Fulfillment of ASSURED criteria compared between different diagnostic methods.

	ELISA	Conventional LFT	2DPN
Affordable	✓	✓	✓
Sensitive	✓	✗	✓
Specific	✓	✗	✓
User-friendly	✗	✓	✓
Rapid and robust	✗	✓	✓
Equipment-free	✗	✓	✓
Deliverable	✗	✓	✓

1.5 Specific Aims and Innovation

In this thesis, we use an electrical circuit model to identify key physical behaviors within a commonly used 2DPN device. We determine critical design principles for this device and introduce an alternative linear network (Pseudo-1DPN) that is similar in appearance to a classic LFT, but can perform the discrete sequential fluid delivery required of a multi-step assay. Additionally, we quantitatively characterize the impact fluid source materials have on reagent release through a strip, a critical tool for identifying appropriate fabrication materials and predicting overall system behavior. To determine the relevance of this circuit based model, we computationally and experimentally explore the behavior of the Pseudo-1DPN format under a variety of different design conditions. Finally, we apply these design capabilities and demonstrate

the utility of this Pseudo-1DPN using an ELISA based assay for detection of acute HIV infections.

Previous work conducted by the Fu/Lutz/Yager group has included using simple electrical circuits to investigate basic fluid transport in strip geometries with multiple width segments during wet-out and after the membrane is fully wetted [50]. This analysis was limited to purely strip based designs, with the goal of providing the framework for understanding fluid flow in a 2DPN. Here, we use this basic framework and expand our analysis to include more complex two-dimensional network shapes. We analyze basic fluid transport in a membrane, as well as the predicted overall fluid delivery behavior in a 2DPN. We largely use this modeling method as a design tool to predict key physical features of a 2DPN and identify how this device platform may be improved.

A Pseudo-1DPN device was previously demonstrated by Samantha Byrnes, Peter Kauffman, and Lisa Lafleur of the Yager Lab. However, this device design was only explored using ideal well sources and was based on their intuition alone. Its behavior was not well understood, making it a controversial device platform. Here, we use electrical circuit modeling to gain a deeper understanding of the physical behavior of this system. Furthermore, we explore its behavior using a variety of different source materials and device geometries to better understand the capabilities and limitations of the system.

Chapter 2: Electrical Circuit Analogues

Over the past few decades, one-dimensional electrical circuit modeling has become a widely used tool for the analysis and design of complex microfluidic systems [56]. While the fluidic behavior of microfluidic devices can be accurately described through mechanical and electrodynamical analysis, this form of device modeling can result in complex systems of partial differential equations that are time consuming and computationally expensive to solve [57]. Circuit modeling, however, has been shown to capture the key characteristics of flow behavior in these networks, while drastically reducing the computational power required [57,58]. Electrical circuit analogies have been used in microfluidic applications that include modeling flowmeters, differentiating cell types based on their electrical properties, detecting cancer cells, culturing stem cells, and altering the local microenvironment of captured cells [59–64]. Here, we use this electrical circuit model to quantitatively describe flow behavior through the porous medium of a 2DPN device. We introduce basic concepts of wicking and demonstrate how electrical models can be constructed for simple networks.

2.1 Fluidic Elements and their Electrical Counterparts

Capillary-driven flow in porous media can be described conceptually by analogy to simple electrical circuits (**Table 2**). Pressure (P) created by capillary force or gravity is represented as voltage (V), viscous resistance (R) is related to properties of the fluid (fluid dynamic viscosity μ) and the permeability (κ) and dimensions of the porous material (cross-sectional area W*H,

wetted length L), and fluid flow rate (Q) is represented by current (I) [65,66]. Atmospheric pressure acts on fluid-air interfaces and is represented as electrical ground at inlets and outlets. The one-dimensional form of Darcy's Law, relates the fluid flow rate to the driving pressure and viscous resistance; it is the equivalent of Ohm's Law in electrical circuits [50,52,67].

Table 2. *Electrical analogy for capillary-driven flow in porous media.*

Electrical Element	Analogous Fluidic Component
Voltage (V)	Pressure (capillary, gravity) (P)
Current (I)	Volumetric Fluid Flow Rate (Q)
Resistance (R)	Resistance (R = $\mu L/\kappa WH$)
Ground (V = 0)	Atmospheric Pressure (P = 0)
Ohm's Law (V = IR)	Darcy's Law (P = QR)

There are two key categories of pressure sources to consider for the general form of a 2DPN – the capillary pressure of the wicking membrane and the backpressure exerted by a fluid source material onto the membrane (P_S). The capillary pressure of the wicking membrane ($P_P = 2\gamma\cos\theta/r$) is constant for a given membrane material and fluid, as the surface tension (γ), contact angle (θ), and membrane pore size distribution (r) are unaltered during device operation. This capillary pressure can be determined experimentally [68]. We find that the backpressure exerted by a fluid source is a significantly more complex element to integrate into a circuit model. This pressure depends on the material used and potentially, the saturation of that material. Fluid delivery through a well is assumed to be 'ideal release,' as the well exhibits a negligible

backpressure on the strip regardless of its fluidic content. Thus, a well is treated as an infinite source and can be represented as 'ground' in an electrical circuit model. In contrast, other source materials, such as fluid delivery pads commonly used in lateral flow tests, may not behave in this same way. These materials may not only exhibit a backpressure during fluid release, but this pressure may vary as a function of their saturation. These non-ideal fluid sources are electrically viewed as voltage sources that have the potential to change over time.

Fluidic resistance through a straight paper channel of constant width is defined as:

$$R = \frac{\mu L}{\kappa WH} \tag{1}$$

For a given strip and fluid, the fluidic dynamic viscosity (μ) and the permeability (κ), width (W), and height (H) of the membrane remain constant. The length of strip wetted by flow (L), however, can be either a constant value or increase with time. If a given region of the device has been completely wet out, none of the above parameters vary and the resistance through that region of the device will be constant. However, if a length of the strip is not completely wet out, the fluid front will progress, causing the wet out length (and resistance) of the strip to increase over time. Here, the changing resistance of the strip is, electrically, visualized as a potentiometer.

2.2 Demonstration of Electrical Circuit Model

To demonstrate the utility of this electrical circuit model, we use it to quantitatively characterize the process of fluid wicking from a finite source into a straight, initially dry strip. For an ideal fluid source, the rate at which fluid wicks through a porous membrane is affected by two opposing forces: 1) the capillary pressure of the material (P_P) that pulls fluid into the strip, and 2)

the viscous resistance (R) that opposes fluid flow through the pores. This resistance will increase as more fluid is taken up by the material and the length of the fluid column increases (**Figure 6A**).

We can describe this time-dependent wicking using an electrical circuit model (**Figure 6B**). We will assume use of an ideal fluid source, represented as electrical ground ($P_S = 0$). Evaluating this circuit, we find that:

$$Q(t) = \varepsilon WH \frac{dL(t)}{dt} = \frac{P_p}{R} = \frac{\kappa WHP_p}{\mu L(t)} \tag{2}$$

and

$$L^2 = \frac{2P_p\kappa}{\mu\varepsilon}t \tag{3}$$

where ε is the void volume of the porous material. The combination of a constant capillary pressure and the rising resistance during wet out causes the progression of the fluid front to slow over time (following $L^2 \sim t$) until the fluid source is depleted (**Figure 6C**). The scaling found in Equation 3 ($L^2 \sim t$) for flow through a porous material matches exactly with the classic Lucas-
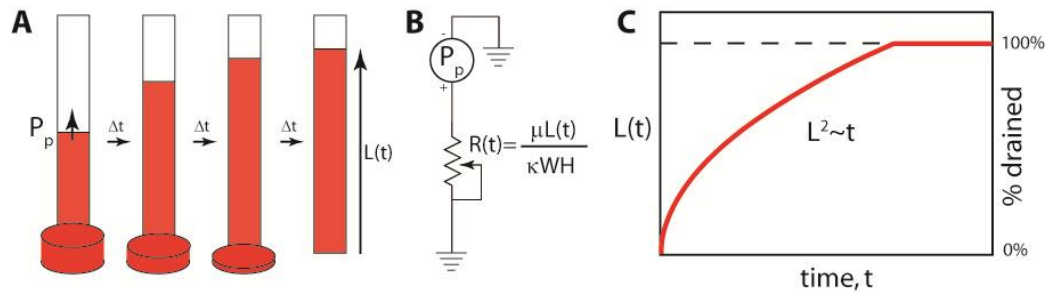
Figure 6. Principles of wicking into simple strips. A) Schematic of wicking into a straight, initially dry strip. Wicking is driven by capillary pressure (P_p) and opposed by viscous resistance to flow through pores that increases as wicking proceeds; the result is a slowing of wicking rate over time. B) An electrical circuit model for wicking into a strip. C) Illustration of migration of the fluid front as a function of time following Equation 3 for a finite fluid source.

Washburn expression describing 1D capillary-driven wet-out through a cylindrical tube [69,70]:

$$L^2 = \frac{\gamma D}{4\mu} t \qquad (4)$$

where γ and D are surface tension and pore diameter, respectively. Thus, electrical analogies can be useful for understanding basic concepts of capillary-driven flow in porous materials [50,52].

Chapter 3: Non-Ideal Fluid Sources

The previous demonstration of using an electrical circuit model to quantitatively understand fluid movement through a porous membrane strip assumed the use of fluid sources that apply negligible backpressure on the strip during release (a condition inherently achieved using well sources). While this simplification offered by wells makes them a well-characterized fluid delivery system, alternative fluid source materials may be better suited for POC settings. For example, LFTs will commonly use a sample pad as a fluid source. Glass fiber pads have been used in 2DPNs to store dried reagents and hold defined volumes of each source fluid (*e.g.,* **Figure 5**), greatly simplifying device implementation. Glass fiber pads were chosen because they release nearly all of their fluid content, but as we find here, what appeared to be an ideal substitute for a well source actually is not.

Fluidic behavior of a device depends not only on the paper network design but also on the release properties of the fluid sources. In this chapter, we characterize the fluid release profiles of several commonly used LFT materials. We show there is a strong relationship between fluid release and the backpressure exerted by a source. This backpressure function can be used as a tool to quantitatively characterize the behavior of a given material and select the material that best achieves the ideal fluid delivery.

3.1 Fluid Release Characterization

Choice of source material can have a dramatic effect on fluid release into a wicking membrane. Here, we explore release from source pads of three different materials commonly used in LFTs and 2DPNs: glass fiber, cellulose, and nitrocellulose.

Methods. Fluid release from a given source was observed by tracking migration of the fluid front through a membrane over time. Nitrocellulose (HF135; Millipore, Billerica, MA), glass fiber (8964; Ahlstrom, Helsinki, Finland), and cellulose (CFSP223; Millipore, Billerica, MA) pads were sized to be saturated by 10 μL of fluid and were individually used to deliver fluid (food dye diluted in deionized water) to an HF135 nitrocellulose membrane of constant size and shape (40 mm x 3 mm) (**Table 3**). Capacity values for glass fiber and cellulose were previously determined by members of the Fu/Lutz/Yager group (Tinny Liang and Peter Kauffman). The capacity of nitrocellulose was measured by comparing the initial mass of a known area of membrane to its mass after saturation. Mass was related to the volume contained using the fluid's density. Materials were housed on adhesive Mylar (10 mil T-5501 Mylar core with 1 mil adhesive on each side; Fraylock, Sancarlos, CA). Overlap between the source pad and nitrocellulose

Table 3. Capacity values of each source material and the pad dimensions used to achieve 100% saturation with 10 μL of fluid.

	Approximate Capacity (μL/cm²)	Pad Dimension (mm x mm)
Glass Fiber	~50	4.4 x 4.4
Cellulose	~70	5.3 x 5.3
Nitrocellulose	~11	10.4 x 10.4

membrane was held constant at 2 mm. All materials were cut to their desired size using a CO_2 laser cutting system (Universal Laser Systems, Scottsdale, AZ). Fluid wet out was recorded using a web camera (Logitech; Fremont, CA) and the position of the fluid front was measured using ImageJ software. Experiments were conducted in a humidity controlled environment (80 – 90% humidity).

Source release profile results. Source material affects not only the total amount of fluid released into the membrane, but also the rate at which fluid is released (**Figure 7**). The length of wicking into the strip is a measure of the volume released. The well case represents perfect delivery. Glass fiber almost completely released its fluidic content (96.8% ± 0.6%), while both cellulose and
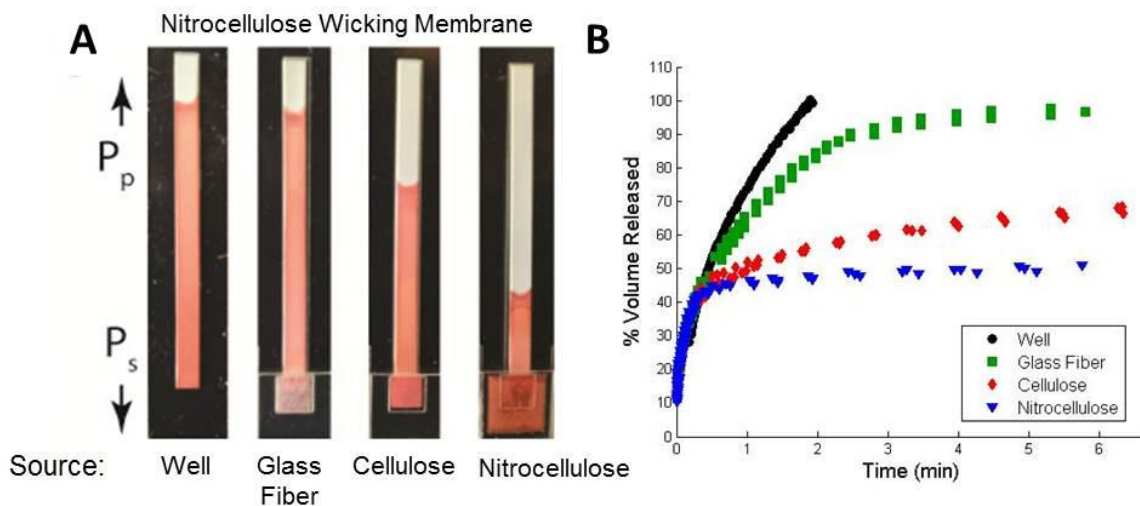
Figure 7. Effects of fluid source materials on capillary-driven fluid delivery into strips. A) Wicking of fluid from different source materials into nitrocellulose strips. Each source was sized to hold the same fluid volume, and images were taken after wicking ceased. The well source can provide complete delivery (100% drained); some materials did not deliver all fluid. The width of each wicking strip is 3 mm. B) Migration of the fluid front during wicking from different source materials. The well case followed the L^2 versus t scaling from Equation 3, while other sources deviated to varying degrees. The percent drained was calculated from L(t) based on the fluid capacity of the nitrocellulose. All data points from n=3 trials (per material) are shown.

nitrocellulose source pads retained a large percentage of their original fluidic load (68% ± 1% and 50% ± 1% fluid released, respectively) (n=3) (**Figure 7A**). The rate of fluid release over time differed between materials as well (**Figure 7B**). As expected, wet out from a well source followed the predicted Lucas-Washburn trend; there is a linear relationship between the square root of time and the length of the fluid column (**APPENDIX I**). While all of the alternative source materials initially followed this trend, the fluid release rates decreased (to different extents) as the pads became less saturated. While glass fiber fully drained, the release rate slowed in comparison the ideal well case. Cellulose delivered an intermediate amount of fluid but showed a much slower release rate. When nitrocellulose was used as both a fluid source and wicking membrane, well-like delivery occurred until the source became approximately 50% depleted, at which point delivery quickly halted.

3.2 Backpressure Characterization

The fluid release curves shown above suggest that a variable, non-zero pressure is applied by a source pad as fluid is drained. Following our electrical analogy, these pads function as voltage sources (rather than the 'ground' shown in **Figure 6**) that oppose the capillary pressure of the wicking membrane (**Figure 8A**). Characterizing the backpressure exerted by the pads should give quantitative insight into the driving force of fluid release from each source.

Derivation of relationship between source backpressure and fluid release. The circuit models for ideal and non-ideal sources can be used to derive an equation that relates the time-dependent

backpressure applied by a given material to experimentally obtainable values (**Figure 6B, Figure 8A**). We describe these networks using simple circuit analysis:

$$\text{Well source:} \quad Q^{well} = \varepsilon WH \frac{dL^{well}}{dt} = \frac{P_P}{R} = \frac{\kappa WH P_P}{\mu L^{well}} \tag{5}$$

$$\text{Nonideal Source:} \quad Q^{pad} = \varepsilon WH \frac{dL^{pad}}{dt} = \frac{P_P - P_S(t)}{R} = \frac{\kappa WH [P_P - P_S(t)]}{\mu L^{pad}} \tag{6}$$

Taking the ratio of these two equations gives the time-dependent applied backpressure of a non-ideal fluid source ($P_s(t)$):

$$\frac{P_S(t)}{P_P} = 1 - \frac{L(t)^{pad} \frac{dL(t)^{pad}}{dt}}{L(t)^{well} \frac{dL(t)^{well}}{dt}} \tag{7}$$

As suggested by the experiments, we see that the capillary pressure of the nitrocellulose and the backpressure exerted by the source material affect both the distance and rate at which fluid travels through the membrane ($L(t)$ and $dL(t)/dt$, respectively). We can further simplify Equation 7 using the porous material form of the Lucas-Washburn equation (previously derived in Chapter 2.2):

$$\left(L(t)^{well}\right)^2 = \frac{2P_p \kappa}{\mu \varepsilon} t \tag{3}$$

to predict the flow profile for the well condition ($L(t)^{well}$ and $dL(t)^{well}/dt$), where γ and D are surface tension and pore diameter, respectively. Grouping the constant term $\frac{2P_p \kappa}{\mu \varepsilon}$ as a newly defined and experimentally obtainable constant, C_{LW}, we can simplify Equation 6 to be:

$$\frac{P_S(t)}{P_P} = 1 - \frac{2L(t)^{pad} \frac{dL(t)^{pad}}{dt}}{C_{LW}} \tag{8}$$

From this equation, we can now quantitatively determine the ratio between the time-dependent backpressure exerted by a source and the capillary pressure of the wicking membrane using just three experimentally obtainable variables – $L(t)^{pad}$, $dL(t)^{pad}/dt$, and C_{LW}.

Methods. It is possible to determine these three unknown variables using the same experimental set-up described in Chapter 3.1. $L(t)^{pad}$ and $dL(t)^{pad}/dt$ are determined by measuring the distance the fluid has wicked through the membrane at a given time. The rate of fluid movement ($dL(t)^{pad}/dt$) is calculated using the equation:

$$\frac{dL(t_i)^{pad}}{dt} = \frac{L(t_i+\Delta t)^{pad} - L(t_i-\Delta t)^{pad}}{2\Delta t} \tag{9}$$

where Δt ranges from 1.8 seconds to 100 seconds. The chosen time step increases with t_i, as migration of the fluid front slows. The Lucas-Washburn parameter defined above, C_{LW}, is determined using the same experimental protocol, with fluid being released from a well rather than from a source pad. Plotting the fluid migration data in the form of length squared versus time, we can extract the value C_{LW} as the slope of the line. This value will be constant for all experiments conducted with a fluid of food dye in water and an HF135 nitrocellulose wicking membrane. The associated Lucas-Washburn coefficient for this condition was determined to be 11.8 ± 0.4 mm^2/sec (n=3) (**APPENDIX I**).

Source backpressure profiles. The backpressure exerted by the three source pads varies as they release fluid (**Figure 8B**). We were unable to collect data points at the point of initial fluid release (percent volume release < 20%) due to a high initial flow rate. However, we predict that all tested materials applied a very low backpressure in the initial stage of delivery (similar to a

well source). This backpressure drastically increased with percent volume depletion, matching the previously observed deviations in fluid release between glass fiber and well sources (**Figure 7B**). The pressure ratio between glass fiber and the wicking membrane ($P_S(t)/P_P$) increased until reaching a maximum value of approximately 0.95 at almost 100% volume depletion. This met our expectation that the pressure exerted by glass fiber was always less than that of the wicking membrane, allowing near complete drainage to occur. In contrast, the backpressures applied by cellulose and nitrocellulose sources increased until they eventually equaled the pressure of the wicking membrane. This occurred once approximately 68% and 50% of their original contents have been released, respectively. The pressure equilibrium eliminated the driving force for flow and as a result, the pads retained the remainder of their fluid (also matching the fluid release behavior seen in **Figure 7B**).
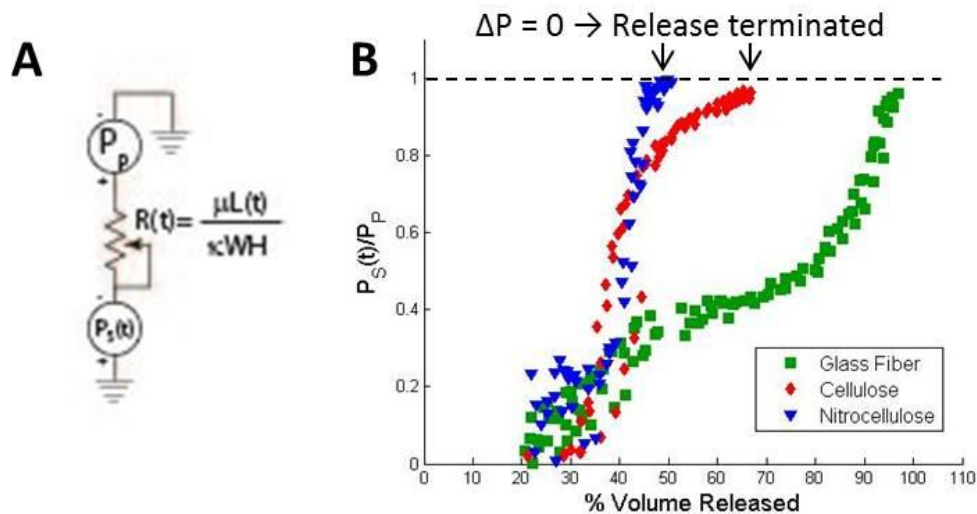
Figure 8. Backpressure effects of non-ideal sources. A) Circuit model for wicking into a strip from a non-ideal fluid source. B) Backpressure profiles during release for different source materials. Profiles were determined from plots in Figure 7B based on Equation 8. The backpressure applied by the source [$P_S(t)$] was normalized to the capillary pressure of the nitrocellulose strip (P_P). Capillary flow stops when this ratio is one. All data points from n=3 trials (per material) are shown.
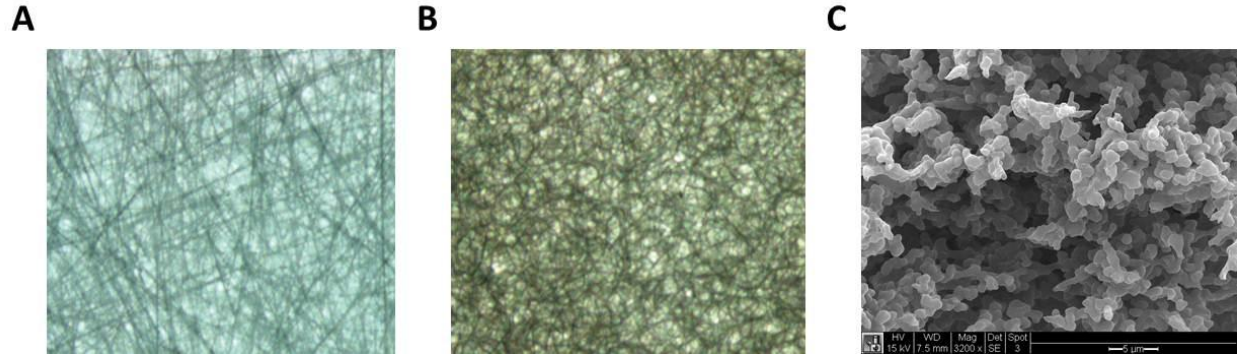
Figure 9. Images of glass fiber, cellulose, and nitrocellulose. *A) Image of Millipore glass fiber conjugate pad at 6.3x magnification. B) Image of Millipore cellulose absorbent pad at 6.3x magnification. C) Scanning electron microscopy (SEM) image of Millipore HF135 nitrocellulose at 3200x magnification. All three materials have a non-uniform pore distribution. We used a different grade of glass fiber and cellulose for our source pads, however, the materials' structures should be similar. [figure sources: A,B) Millipore product manual. Hi-Flow Plus Membranes and SureWick Pad Materials, C) Gina Fridley, Yager Lab]*

The capillary pressure of a source material is inversely related to its pore size ($P_{cap} = 2\gamma\cos\theta/r$). Since many potential source materials have a non-uniform pore distribution, it is not surprising that the backpressure applied by the source changes during drainage. For example, a material composed of small and large pores may apply a bimodal backpressure. The pressure may first be low as the large pores drain, but then increase when only the small pores remain filled. Glass fiber, cellulose, and nitrocellulose all have non-uniform pore distributions (**Figure 9**).

In the following chapters, we describe the impact of ideal and non-ideal fluid sources on paper network behavior. We incorporate the backpressure function of a glass fiber source pad into an electrical circuit model to represent a device system that utilizes non-ideal sources. To quantitatively define glass fiber's variable pressure curve, we fitted it to a third order polynomial function ($R^2 = 0.9704$):

$$\frac{P_S(t)}{P_P} = -5.78\alpha(t)^3 + 7.81\alpha(t)^2 - 3.92\alpha(t) + 1.06 \qquad (10)$$

where $\alpha(t)$ is the fraction of volume still remaining in the pad. This will later be used to fill in the previously unknown voltage source values associated with a given non-ideal fluid source.

3.3 Conclusions

In this chapter, we found that the choice of source material in a device has a dramatic effect on both the total percent of fluidic content released over time and the rate of delivery. All three source materials were found to exert a backpressure on the wicking membrane that varies as a function of their saturation. We attribute variations in fluidic delivery to these differences in applied backpressure.

Because it is completely depleted, glass fiber has previously been chosen as a suitable replacement for a well source. Here, we found that there are actually fundamental differences in the behaviors of these sources. The non-negligible backpressure exerted by a glass fiber source causes the rate of fluid release into a membrane to deviate from that achieved using a well.

Chapter 4: Application of Electrical Circuit Models

The Fu/Lutz/Yager Group at the University of Washington has successfully developed numerous 2DPN devices that are capable of performing multi-step diagnostic assays and achieving a clinically relevant limit of detection (LOD). While these devices achieve their overall detection goal, their fluidic behavior is often not well understood or characterized. This lack of understanding can cause the device design process to: 1) be tedious, as design is based largely on an "estimate and check" method, 2) be non-robust, with designs needing to be altered based on assay requirements (number of reagents, volume of each delivery step, *etc.*), and 3) result in a non-optimal overall design, as critical parameters such as binding rates and exposure times between reagents may not be fully considered or easily accounted.

In this chapter, we seek a basic understanding of the behavior of a specific 2DPN by applying electrical circuit analogies to its fluidic components. We use this modeling method to define systems of basic equations that relate device parameters to volumetric flow rates in the device. We identify key design principles for this previously-developed 2DPN and introduce an alternative linear paper network (Pseudo-1DPN) that takes advantage of system-level behavior to perform discrete, sequential reagent delivery. For simplicity, we initially illustrate device principles using a 2DPN with two fluid sources. This is expanded in future chapters to include additional delivery steps.

4.1 Two-Dimensional Paper Network

We analyze the network behavior of a previously-developed 2DPN to develop a quantitative understanding of fluid release throughout the device. Specifically, we focus on the effects of device design parameters on flow behaviors/source fluid release rates.

The network behavior for sequential fluid delivery in a 2DPN is demonstrated using a device with two legs of equal length (two delivery steps) and non-ideal fluid sources (**Figure 10A**). We divide the release behavior of this device into two distinct stages. The first stage occurs after an initial wet-out period, in which the two fluids meet in the spacer region mid-way between the two legs (**Figure 10A, left**). During this first stage, both sources have the potential to release fluid into the wicking membrane. The second stage of the device occurs once the rightmost source (S_1) has been depleted of its contents; only the leftmost source (S_2) continues to deliver fluid in this stage.

We can convert the two stages of operation in this complex device into relatively simple electrical circuits using the analogies outlined in Table 2 (**Figure 10B**). The wicking membrane and two fluid sources are viewed as three separate voltage sources. The voltage associated with the wicking membrane (P_P) is constant over time, while the voltages associated with the non-ideal sources ($P_{S1}(t)$, $P_{S2}(t)$) have the potential to vary. The fluidic resistance of the membrane is represented by either a resistor or potentiometer, depending on whether or not the region is fully wetted. In the first stage of delivery, voltages associated with both fluid sources are present
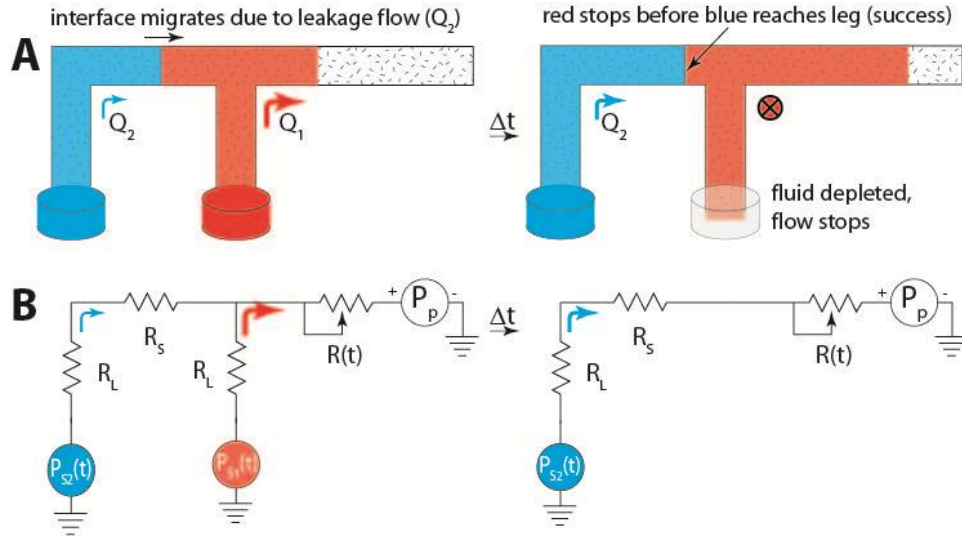
Figure 10. Network behavior for sequential delivery in a 2DPN. A) After initial wet-out occurs, fluid will continue to flow through both legs, which causes the fluid interface to migrate. Successful sequential delivery occurs if the red fluid drains completely before the blue fluid reaches its leg. B) Circuit model for the two stages of delivery in the 2DPN.

(**Figure 10B, left**). However, once S_1 is completely drained and no longer making a fluidic contribution to the system, its respective voltage is no longer considered (**Figure 10B, right**).

We can use mesh and nodal analysis to translate these electrical circuit models into equations that re late current (or flow rate) to the voltage and resistance throughout the device. In the first stage of the device, fluid should be released from the two sources at rates of:

$$Q_1 = \frac{P_P[R_L+R_S] - P_{S1}[R_L+R_S+R(t)] + P_{S2}R(t)}{R(t)[2R_L+R_S] + R_L[R_L+R_S]} \tag{11}$$

$$Q_2 = \frac{P_{S1} - P_{S2} + Q_1R_L}{R_L+R_S} \tag{12}$$

Once the rightmost source is completely drained of fluid, the rate of release from S_2 changes to:

$$Q_2 = \frac{P_P - P_{S2}}{R_L+R_S+R(t)} \tag{13}$$

The surprising complexity of these equations demonstrates the difficulty of predicting fluid behavior within a device from intuition alone. There is a non-linear relationship between device geometry and flow rate. Additionally, source pressure, which we have previously shown to potentially be a dynamic variable that changes as a function of source saturation, plays a critical role in device behavior. Applying electrical circuit analogies to this device, however, makes it a relatively straightforward process to simplify the system in a set of well-defined equations.

In the first stage of the device, we see that both Q_1 and Q_2 are potentially non-zero; both sources may continue to deliver fluid after the initial wet-out period, but at different rates. This "leakage" flow (Q_2) causes migration of the blue fluid front as the red fluid is still being delivered (as seen in **Figure 10A**). Successful sequential delivery would require that the first fluid (red) is completely drained before arrival of the blue-red fluid front (as depicted in **Figure 10A**). In other words, delivery is "clean" if the time for depletion of S_1 (T_{drain}) is shorter than the time for migration of the leakage front to reach the right leg junction (T_{mig}). A quantitative criterion for success must also consider the volumetric capacity of the spacer region (*i.e.*, the region can be filled by the flow Q_2 before failure). Unsuccessful design results in both fluids flowing into the detection leg in parallel (*e.g.*, yellow and clear fluids in **Figure 4**) and/or fluid mixing.

Leakage flow, or front migration, may have an insignificant impact on sequential delivery if the device is designed with this non-ideality in mind. Migration can be accounted for using an "estimate and check" method, which potentially requires multiple iterations of device fabrication until desired behavior is achieved. Alternatively, it is possible to identify key design criteria for

achieving successful sequential delivery using only the above system equations to better understand the relationship between leakage flow and device geometry. To highlight the importance of device geometry on this migration, we will simplify the previously defined device to assume use of ideal fluid sources ($P_{S1} = P_{S2} = 0$ Pa). The fluidic behavior of the device after initial wet-out (when leakage flow may occur) is now described as:

$$Q_1 = \frac{P_P[R_L+R_S]}{R(t)[2R_L+R_S]+R_L[R_L+R_S]} \tag{14}$$

$$Q_2 = \frac{P_P R_L}{R(t)[2R_L+R_S]+R_L[R_L+R_S]} \tag{15}$$

Taking the ratio of these two flow rates allows us to define a term that describes the magnitude of this leakage flow during the first stage of operation:

$$\frac{Q_2}{Q_1} = \frac{1}{1+{R_S}/{R_L}} \tag{16}$$

The ratio of flow rates delivered by each leg is a critical parameter in achieving device success; we find that it can be determined solely by the resistances in the network. Ideally, this ratio would be zero in the first stage of delivery, with no fluid release occurring from S_2 (blue, Q_2) as S_1 (red, Q_1) drains. From Equation 16, we see that, given this 2DPN device design, it is impossible to eliminate leakage flow even with ideal sources. However, migration effects can be minimized by either increasing the resistance of the spacer region (R_S, *e.g.*, by increasing length or decreasing width) or decreasing the resistance of the delivery legs (R_L, *e.g.*, by decreasing length or increasing width). An example of how a 2DPN device may be redesigned in consideration of these results can be seen in Figure 5; the reagent delivery legs were drastically shortened in

33

comparison to the first generation device depicted in Figure 4 to decrease their associated resistance and reduce leakage flow.

This model demonstrates that there is an inherent shortcoming to this commonly utilized 2DPN device design – all sources within a device release their fluids at the same time, potentially causing issues in sequential reagent delivery. This leakage behavior can be reduced by altering device design, but can never be completely eliminated. Electrical circuit models of the system predict that reducing the resistance associated with each delivery leg has a significant impact on front migration during the initial delivery stage. This finding leads us to a critical design prediction – complete elimination of delivery legs should improve sequential delivery.

4.2 Pseudo-One Dimensional Paper Network

We can completely eliminate delivery legs within the above 2DPN by placing all fluid sources directly onto a linear strip; we refer to this new device as a Pseudo-One Dimensional Paper Network (Pseudo-1DPN) (**Figure 11A**). As expected, the circuit models for this system closely resemble those associated with the 2DPN (**Figure 11B,C**). The only deviation is the absence of all R_L resistors (in analogy to the removal of delivery legs).

The initial stage of sequential delivery in a Pseudo-1DPN is defined with the equations:

$$Q_1 = \frac{P_P - P_{S1}}{R(t)} \tag{17}$$

$$Q_2 = \frac{P_{S2} - P_{S1}}{R_S} \tag{18}$$

$$\frac{Q_2}{Q_1} = \frac{R(t)[P_{S1} - P_{S2}]}{R_S[P_P - P_{S1}]} \tag{19}$$
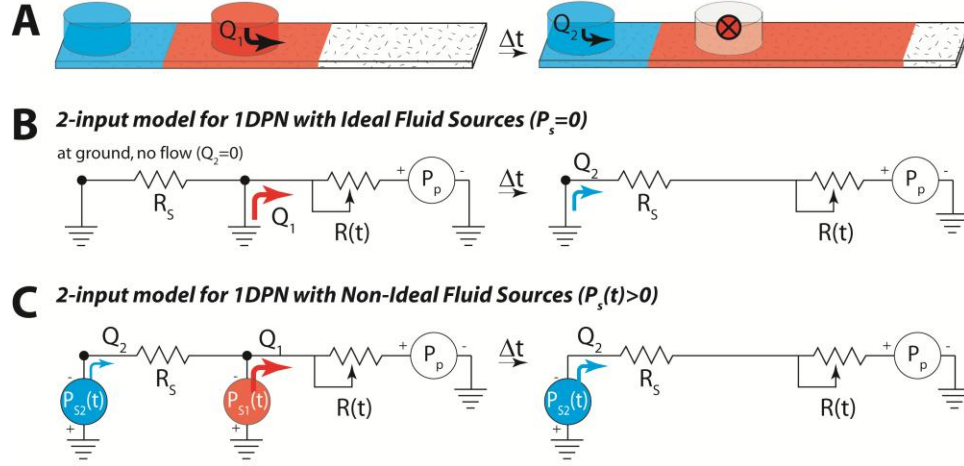
Figure 11. Network behavior of two-step sequential delivery in a Pseudo-1DPN using ideal and non-ideal fluid sources. *A) If ideal sources are used, the fluid front of the left fluid (blue) will remain stationary until the right source (red) is completely drained. Only then will the left source (blue) release its contents. B) A circuit model for sequential delivery in a Pseudo-1DPN that uses ideal fluid sources. C) A circuit model for sequential delivery in a Pseudo-1DPN that uses non-ideal fluid sources. Fluid will be released from both sources simultaneously, allowing a potential for leakage to occur (similar to the 2DPN device).*

Once S_1 (red) has been drained, the flow rate from S_2 (blue) is:

$$Q_2 = \frac{P_P - P_{S2}}{R_S + R(t)} \tag{20}$$

The systems equations for a Pseudo-1DPN are markedly less complex than those of the 2DPN. Flow rate throughout the system is largely dependent on the pressures exerted by the wicking membrane and fluid sources, and the fluidic resistance of the spacer region between sources. Initially, the flow rate of fluid from the left source is a function of the pressure differential between the two sources and the spacer resistance. Thus, the potential for leakage to occur depends entirely on the backpressure applied by the source material and how it changes as fluid is drained. These two factors are highly variable between different types of materials (as shown in

Chapter Three). As with the 2DPN above, leakage can also be mitigated by increasing the spacer resistance.

Choice of source material plays a critical role in achieving successful sequential delivery with a Pseudo-1DPN device. Using the above equations, we can predict the system's behavior and likelihood of success given the use of three different classes of source materials: 1) ideal sources that exhibit negligible backpressure, 2) non-ideal sources that exhibit constant, non-negligible backpressure, and 3) non-ideal sources that exhibit variable, non-negligible backpressure.

Ideal sources (P_{S1} = P_{S2} = 0). For the case of ideal sources (*e.g.*, a well or large diameter capillary), we can say that their exerted backpressure is zero (if we ignore the force of gravity acting on the fluid column, an assumption that is further discussed in Chapter 5) (**Figure 11B**). By Equation 19, there should be no leakage flow in the system, since there is no pressure difference between the two fluid sources. Therefore, we predict that ideal sources will give discrete sequential delivery even for small spacing between fluid sources (small R_S). This is an extremely useful device characteristic as it will allow both reagent waste and device run time to be minimized. Additionally, the driving force (P_P – P_{Source}) for reagent delivery through the device (*e.g.*, delivery of the right fluid in the first stage of delivery and the left fluid in the second stage of delivery) will depend only on the capillary pressure of the wicking membrane.

Non-ideal source with constant backpressures. Similarly to an ideal source, non-ideal sources that exert a constant, non-zero backpressure are expected to always achieve successful sequential delivery in a Pseudo-1DPN, regardless of the spacing distance between sources. The pressure

exerted on the wicking membrane is constant regardless of material saturation, and thus, there is no pressure differential between sources. The only difference in system behavior between devices using these non-ideal sources or ideal sources is the magnitude of the driving force for reagent delivery (and thus the device run time). If we compare two devices that are of the same dimension and differ only in their source type, the device with the non-ideal source will have a slower flow rate because the pressure gradient is now reduced by the backpressure exerted by the source ($P_P - P_{Source}$). The magnitude of this difference will depend entirely on the significance of the source backpressure. If the source backpressure is similar in magnitude to the capillary pressure of the wicking membrane, we would expect to see a very slow flow rate throughout the system. However, if the source backpressure is low in comparison to the pressure of the wicking membrane, we may see little difference in flow rate between devices with ideal or these non-ideal sources.

Non-ideal sources with variable backpressures. The fluidic behavior of a Pseudo-1DPN becomes significantly more complex when considering use of non-ideal sources that exert a variable backpressure on the wicking membrane (**Figure 11C**). As we have seen in Chapter Three, many of the materials commonly used in LFTs and 2DPNs (glass fiber, cellulose, nitrocellulose) behave in this way, making it a non-trivial category that must be considered.

Fluid flow rates from S_1 and S_2 are not equivalent; sources release fluids at different rates and will be at different saturation levels at a given time (Equations 17 and 18). This can translate into different backpressures exerted on the membrane and thus, a pressure differential between

sources. This resulting pressure differential serves as the driving force for leakage flow to occur from S_2. The magnitude of front migration will largely be affected by the choice of source material (and its associated backpressure curve) and the stage of the device. For example, we have seen that in the case of a nitrocellulose source pad, the backpressure is relatively low and non-variable at high saturation values, but dramatically increases once the pad is approximately 40% drained. Thus, we can predict that in the initial stage of the device when the nitrocellulose pads contain a large percentage of their original volumes, there will be minimal leakage of the leftmost fluid. However, once the rightmost fluid has released approximately 40% of its fluids, the pressure differential between pads, and thus leakage flow, will drastically increase. The significance of leakage flow caused by materials with a more complex backpressure function, like glass fiber and cellulose, is difficult to predict based on intuition alone.

4.3 Conclusions

In this chapter, we used electrical circuit modeling to identify an inherent limitation of a commonly used 2DPN device design. It is impossible to completely eliminate premature fluid release from the sources. However, reducing the resistance associated with the delivery legs should decrease the magnitude of leakage flow in the device. This led us to the design prediction that eliminating delivering legs from the 2DPN device design (creating a Pseudo-1DPN) would allow for improved sequential delivery.

A Pseudo-1DPN device design had previously been demonstrated by Lisa Lafleur, Samantha Byrnes, and Peter Kauffman of the Yager Lab. However, its behavior was not well understood.

Here, through electrical circuit modeling, we were able to gain a deeper understanding of the physical behavior of this system. Analysis of the Pseudo-1DPN system leads us to three key design principles: 1) we can achieve discrete sequential delivery, regardless of the spacing between sources, if the device uses sources that exert a constant or negligible backpressure, 2) it is critical to consider the backpressure curve of a non-ideal source material, as it will greatly affect the extent of leakage flow that occurs in the device, and 3) leakage flow caused by variable, non-ideal sources can be accommodated by increasing the spacer resistance between sources.

Chapter 5: Computational Modeling of a Pseudo-1DPN

In the previous chapter, we used an electrical circuit model to identify a promising new device design, a Pseudo-1DPN. We mathematically defined fluid flow rates throughout this device using a set of basic algebraic equations and were able to predict key device behaviors given a variety of device parameters. To further explore the predictive capabilities of this model, we expand these analytical solutions into a computational model that is able to track device performance over time. This computational systems model can potentially be used for three major functions: 1) provide a visual representation of the predicted behavior of the system (*i.e.* flow rate as a function of time, the significance of leakage flow in a device, *etc.*), 2) serve as a tool for determining if the electrical circuit model captures the key physical behavior of the system, and 3) serve as a design tool for developing devices that achieve the desired fluidic behavior.

In this chapter, we translate our previously developed analytical model into a computational systems model. We explore device behavior both experimentally and as predicted by this model under a variety of experimental conditions; source type and device geometry are both varied. These results are not used to thoroughly validate this model; they will be used as a tool to determine if the electrical circuit model captures the key physical behavior of the system under a wide range of design conditions.

5.1 Methods

To improve the relevance of this device system, we expand our model to include three reagent delivery steps within a Pseudo-1DPN. The analytical model for this new system is defined in a similar manner as was shown in Chapter Four (**Figure 12**). Again, we only consider fluid flow after initial wet-out has occurred (fluids have met in the middle of each spacer region); this serves as our initial condition. We must now consider three major reagent delivery stages: 1) all three pads contain fluid, 2) the rightmost source has been depleted, while the other two sources still retain some volume, and 3) only the leftmost source contains fluid. The analytical equations that describe fluid release from sources during each device stage closely resemble those previously derived in Chapter 4.2 and can be seen in **APPENDIX II**.
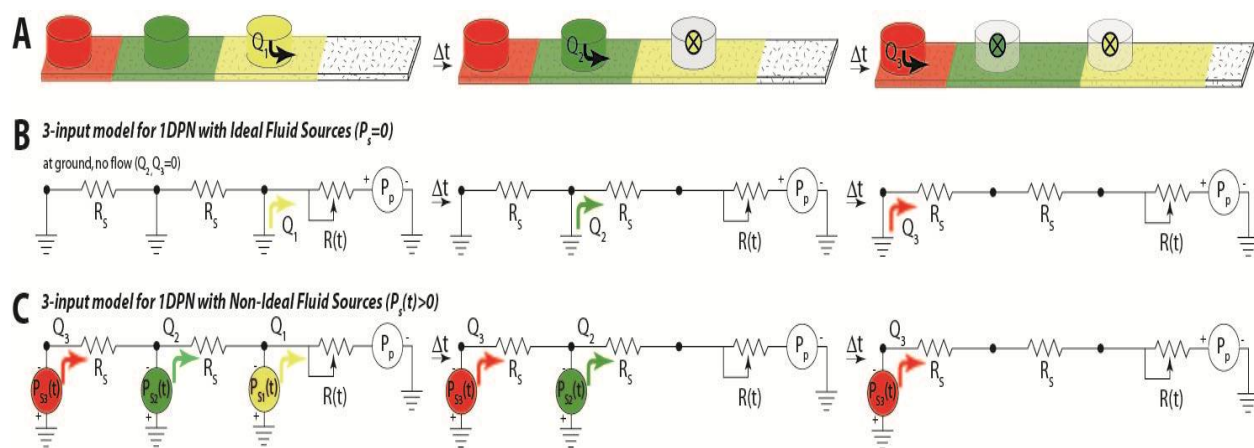
Figure 12. Network behavior of three-step sequential delivery in a Pseudo-1DPN using ideal and non-ideal fluid sources. A) If ideal sources are used, the fluid front of the second (green) and third (red) sources will remain stationary until the right source yellow) is completely drained. Only after the previous source is drained will a given source release its contents. B) A circuit model for sequential delivery in a Pseudo-1DPN that uses three ideal fluid sources. C) A circuit model for sequential delivery in a Pseudo-1DPN that uses three non-ideal fluid sources. Fluid will be released from both sources simultaneously, allowing a potential for leakage to occur (similar to the 2DPN device).

Analytical equations can be used to create a computational model that tracks the behavior of the system over time. The membrane resistances and potentially the source backpressure terms included in the derived systems equations are time-dependent. As a result, flow rates through the device will change over time, based on the progression of the system. We use this computational model to track this system progression and subsequently, calculate fluid release rates. We explore device behavior given a variety of different design parameters (ex. altered source material, geometry). Experimentally, we can fabricate these specific devices and quantitatively characterize fluid release into the device. We compare device behavior, as predicted by the model, to the experimentally obtained results to shed insights into the validity of this electrical circuit model for porous medium.

Computational model methods. All computational simulations of a Pseudo-1DPN were performed using MATLAB R2012a. **Figure 13A** provides a schematic of the modeled Pseudo-1DPN with all relevant sources and dimensions labeled; sources are labeled in increasing order, starting from the source that would deliver fluid over a theoretical capture line first. An overview of necessary system parameters and variable is given in **APPENDIX III**. The computational model was developed in three major stages: define relevant system parameters, define initial conditions, and track system progress over time. A flow chart summarizing the implementation process of the computational model is shown in **Figure 13B**.

We defined the inherent properties of the wicking membrane and fluid using values determined experimentally or from literature. Tunable device design parameters were initially chosen in

consideration of previously demonstrated 2DPN devices; these parameters can be easily altered to fit the system of interest.

We considered system behavior only after initial wet out occurred; some amount of fluid was
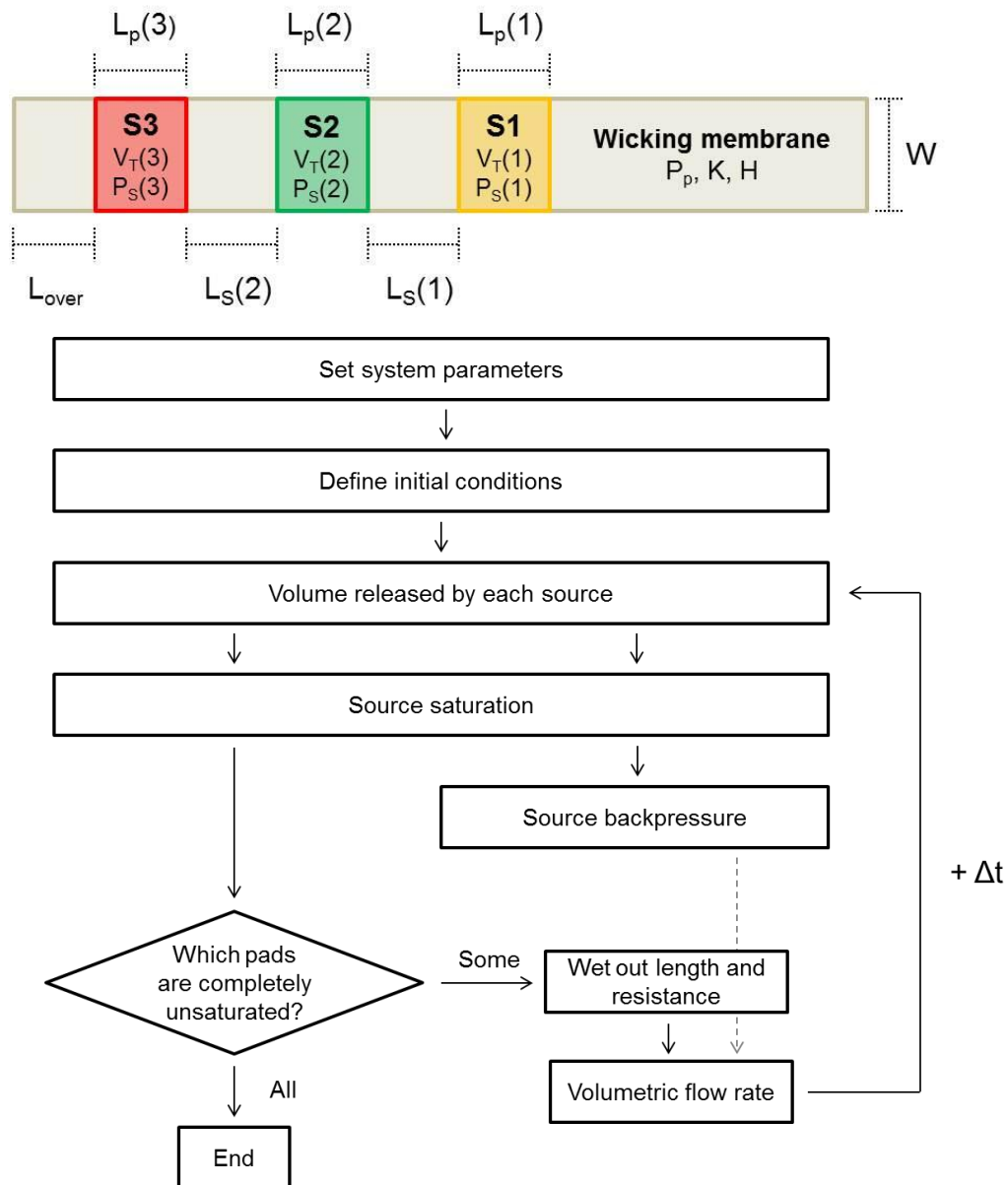
Figure 13. Computational model design for a Pseudo-1DPN with three delivery steps. A) Schematic of modeled device with critical system parameters labeled. B) Flow chart that outlines the overall implementation process for determining the fluidic behavior of the Pseudo-1DPN in MATLAB.

already released from the sources and sections of the membrane were either partially or fully wetted. We assumed fluid from two neighboring sources met midway between their spacer region and that fluid traveled the same distance to the right of S_1 as it did to the left. We used these wet out distances to calculate the resistance of each membrane region and the volume released by each source. From these values, we could determine the backpressure exerted by each source and the initial rate of fluid release from each source. This set of values served as the initial condition for device operation. We calculated this same set of variables at each point in time (with time increments of 1 second) to describe the system's behavior. A detailed description of the model is provided in **APPENDIX IV** and the full MATLAB code for flow in a Pseudo-1DPN is shown in **APPENDIX V**.

Experimental methods. To determine the relevancy of this circuit based model, computationally modeled Pseudo-1DPNs were experimentally developed as well. HF 135 nitrocellulose was used as the wicking membrane and placed on an adhesive Mylar sheet (10 mil ACA). Devices used one of two different source types: thick glass fiber pads and capillaries with a 2 mm diameter (CV2024; Vitrotubes, Mountain Lakes, New Jersey). Glass fiber pad sources were positioned and brought into contact with the membrane using a folding adhesive Mylar card; saturated fiber pads were placed on one side of the card, with the nitrocellulose wicking strip on the other. The card was folded to activate the device. To achieve the desired spacing distance between capillary sources, a capillary holder was fabricated from poly(methyl methacrylate) (PMMA). The holder was mounted to a precision stand and a rubber band was
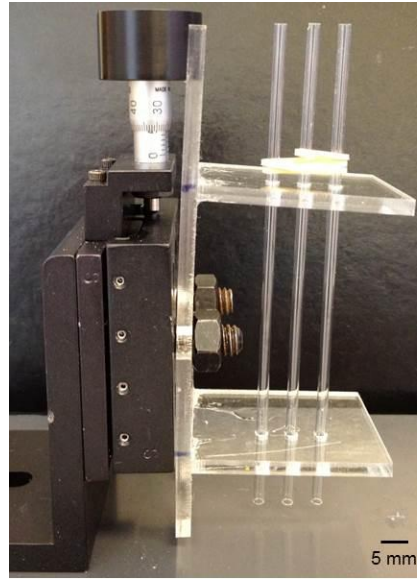
Figure 14. Capillary stand fabricated to achieve desired tube positions. The tube holder was used to set the spacing distance between capillaries. A rubber band was wrapped around the tubes and the holder was mounted to a precision stand to ensure all sources made contact with the nitrocellulose membrane at the same time.

wrapped around the set of capillaries to ensure all sources make contact with the membrane at the same time (**Figure 14**). All experiments were performed at approximately 90% humidity. A web camera was used to capture fluid release from the device; a frame rate of 5 frames/sec was used for approximately the first 90 seconds of device operation and was subsequently decreased to 1 frame/sec. Food dyes of different colors (diluted in water) were used for each source.

For all capillary based experiments (n=3), wet out lengths were tracked using ImageJ. This was used to calculate the percent of fluid released and flow rate of each source over time (as described in Chapter 3.3); flow rate was calculated using the equation:

$$\frac{dV(t_i)}{dt} = \frac{V(t_i + \Delta t) - V(t_i - \Delta t)}{2\Delta t} \tag{21}$$

Time steps (Δt) of 5, 10, and 20 seconds were used for Sources 1, 2, and 3, respectively. There was a degree of imprecision using this data analysis method; complex, non-uniform fluid fronts

made it difficult to precisely and accurately determine wet-out length and there was inherent error associated with manually measuring these lengths. These potential deviations could significantly impact flow rate results, especially given low flow conditions. Larger time increment values were chosen for sources associated with lower flow rates to reduce the effects of this error.

5.2 Pseudo-1DPN with Glass Fiber Sources

Though glass fiber is a widely used source material in LFTs, the changing backpressure it applies on the nitrocellulose membrane during drainage has the potential to cause issues of premature flow and leakage in this Pseudo-1DPN. We explore sequential delivery in a Pseudo-1DPN with non-ideal, glass fiber pad fluid sources to understand the significance of this leakage flow (**Figure 15A**). Analysis of this device is purely qualitative, as the model was unable to account for effects of fluid migration through downstream source pads; this migration likely impacted source saturation and fluidic resistance over time. The device system consisted of three 4.4 mm x 4.4 mm pads, each holding 10 µL of fluid, spaced 5 mm apart. The HF135 membrane had a width of 4 mm, and L_{over} was zero.

Initial simulations involving three-step sequential delivery matched our expectation that premature flow would occur between the pads (**Figure 15B,C**). As fluid from the right-most pad (clear) was released, fluid drained from all other sources as well. Sources 1 and 2 became depleted at approximately the same time, at which point Source 3 had already released the majority of its content (~80%) (**Figure 15B**). After initial wet out occurred, the flow rates of Sources 2 and 3 immediately rose to values comparable to that of release from Source 1 (**Figure 15C**). This

leakage flow was caused entirely by the pressure differential between sources. Thus, although glass fiber is able to almost completely release its fluidic load, its saturation–dependent backpressure has the potential to dramatically worsen sequential delivery in a Pseudo-1DPN.

Experimentally, this significant leakage flow was found to cause device failure (**Figure 15D**).
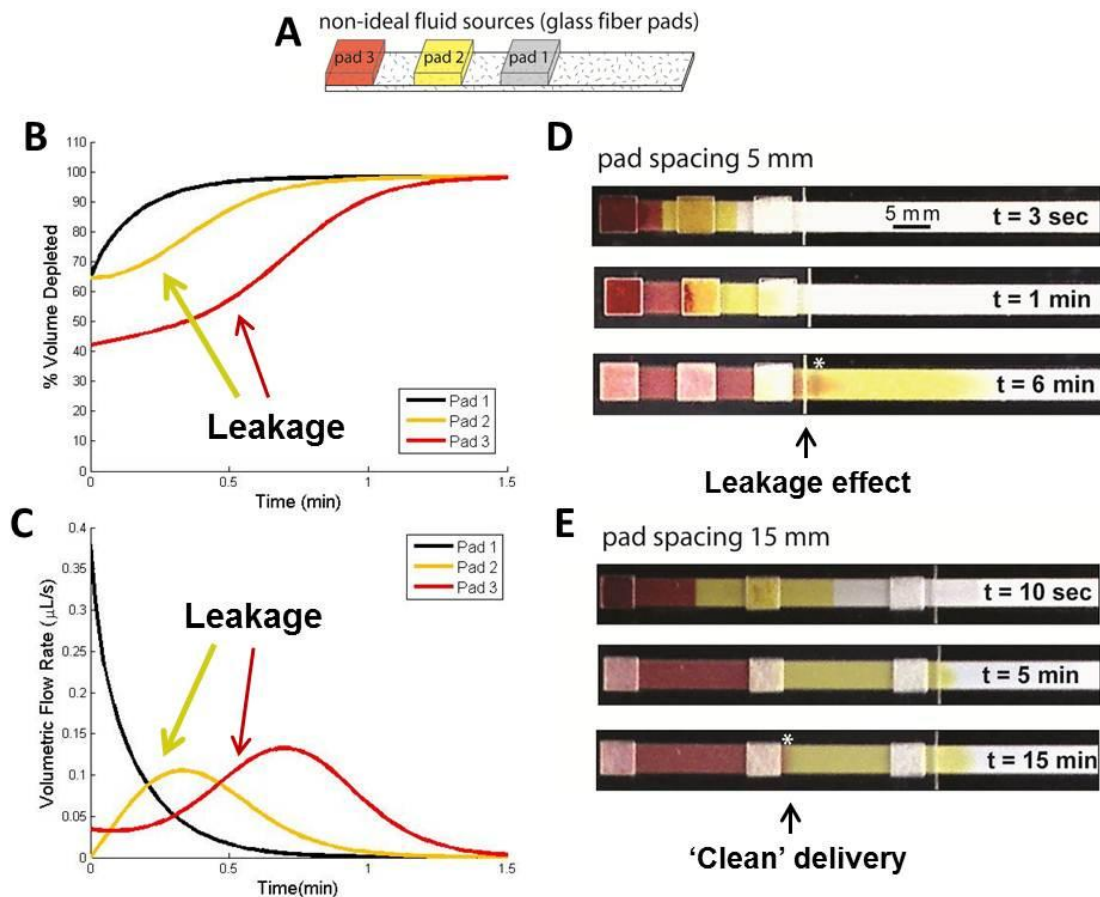
Figure 15. Model behavior and results for devices with non–ideal sources (glass fiber pads). *A) Schematic of a 3-source Pseudo-1DPN that uses glass fiber pads to deliver clear, yellow, and red fluids. B) Computational model results for percent fluid release over time from all sources in the Pseudo-1DPN (L=5mm). C) Computational results for volumetric flow rate of fluid release from all sources (L=5mm). The model of this scenario predicts that both the yellow and red fluids will be prematurely released. D) Time-lapse images of failed sequential delivery. High leakage flow (due to small spacer resistances (L=5 mm)) resulted in mixing and non-uniform fluid interfaces. E) Time-lapse images of successful sequential delivery. Increased spacer resistances (L=15 mm) accommodate fluid leakage so that clean delivery was still achieved. No mixing occurred in the glass fiber pads and there was a distinct interface between the different fluids. Each pad delivered 10 microliters (30 microliters total for three sources).*

Initial wet-out occurs soon after device activation. However, after wet-out, fluids from the second and third pads continued to migrate, reaching the next pad before it completely drained. This caused unwanted mixing to occur in both the glass fiber pad (noticeably seen at t = 1 min) and the nitrocellulose membrane (exhibited by the long red fluid front seen at t = 6 min, marked by *).

As was the case of the 2DPN, issues caused by this leakage flow could be avoided with appropriate device design. The circuit model from Chapter 4 showed that increasing spacer resistance decreases the flow ratio between sources and improves the likelihood of device success. **Figure 15E** shows time-lapse images of a Pseudo-1DPN that was able to achieve clean delivery with an increased pad spacing distance of 15 mm. No obvious mixing of fluids occurred in either the pads or at the fluid boundaries. While the fluid front of the red fluid stopped somewhat beneath Pad 2, there still appeared to be a relatively clear distinction between the red and yellow fluids (marked by *).

5.3 Pseudo-1DPN with Capillary Tube Sources

Previous analytical model predictions lead us to believe that use of ideal sources result in entirely discrete sequentially delivery in a Pseudo-1DPN. To test this prediction, large-diameter capillary tubes (d = 2mm) were used as near ideal sources. Slight non-idealities arise due to two conflicting pressures (capillary and gravitational pressures), which cause the tubes to exert some amount of backpressure onto the wicking membrane. Capillary pressure allows fluid to be taken up by the source and is constant for a given tube size, fluid, and contact material. Gravitational pressure is a

function of the height of fluid in a tube; this pressure decreases as a vertical tube releases its content. Theoretically, a capillary tube should function as a variable pressure source.

For completeness, we included both the effects of source capillary pressure and gravitational pressure in our computational model. However, for our system, we determined that the backpressure exerted by a capillary tube source is negligible in comparison to the capillary pressure of the nitrocellulose wicking membrane (**APPENDIX VI**). Thus, realistically, a capillary tube should function similarly to an ideal well source.

Here, we used a device with capillary tube sources spaced 4.25 mm apart on a 4 mm wide nitrocellulose wicking membrane. The L_{over} distance was 2.13 mm and each fluid source was initially supplied with 15μL colored H_2O.

Computational and experimental results. Both the computational and experimental results for this system matched our prediction that fluid release from each source largely begins only after the previous source has been completely drained (**Figure 16**). The model predicted that each source released approximately 19% of its original fluidic content during initial wet out. Experimental results closely matched this prediction, providing support for our definition of initial wet out (**Table 4**). Experimentally, the slightly larger amount of volume depleted from Source 1 (in comparison to the other two sources) was likely due to a minor time offset in the true Time Zero, caused by an insufficient camera frame rate. We later find that the initial volumetric flow rate of fluid from Source 1 is relatively high, meaning that small time discrepancies could lead to noticeable anomalies in fluid release.

Table 4. *Percent volume released by each fluid during initial wet out (n=3).*

	Volume Released (Computational)	Volume Released (Experimental)
Source 1	19%	22% ± 1%
Source 2	19%	19% ± 1%
Source 3	19%	17.9% ± 0.5%

After initial wet-out, Source 1 released fluid at a relatively fast rate, while Sources 2 and 3 largely retained their load. As predicted by the Lucas-Washburn equation, the rate of fluid release from this first source was not constant, but decreased as the wet-out length increased. In later stages of delivery, this same decrease in flow rate over time was evident with Sources 2 and 3 as well.

There was a significant decrease in the overall fluid release rate of each source as delivery progressed. This was due the increasing length of membrane wet out and the additional resistances between sources. As a result, Sources 2 and 3 had much lower flow rates than that of Source 1. The delivery time required to drain each source drastically increased between Sources 1, 2, and 3 (**Table 5**). While this trend may seem insignificant, practically speaking, it may have a great impact on the performance of a diagnostic assay, the true goal of this device. Assuming equal source volumes are used, the first reagent will be delivered at a high flow rate, for a short time. Interaction time between the reagent and a capture line will be limited and may be inadequate for achieving sufficient binding. Thus, additional design considerations may need to be made to reach the desired level of binding between reagents.
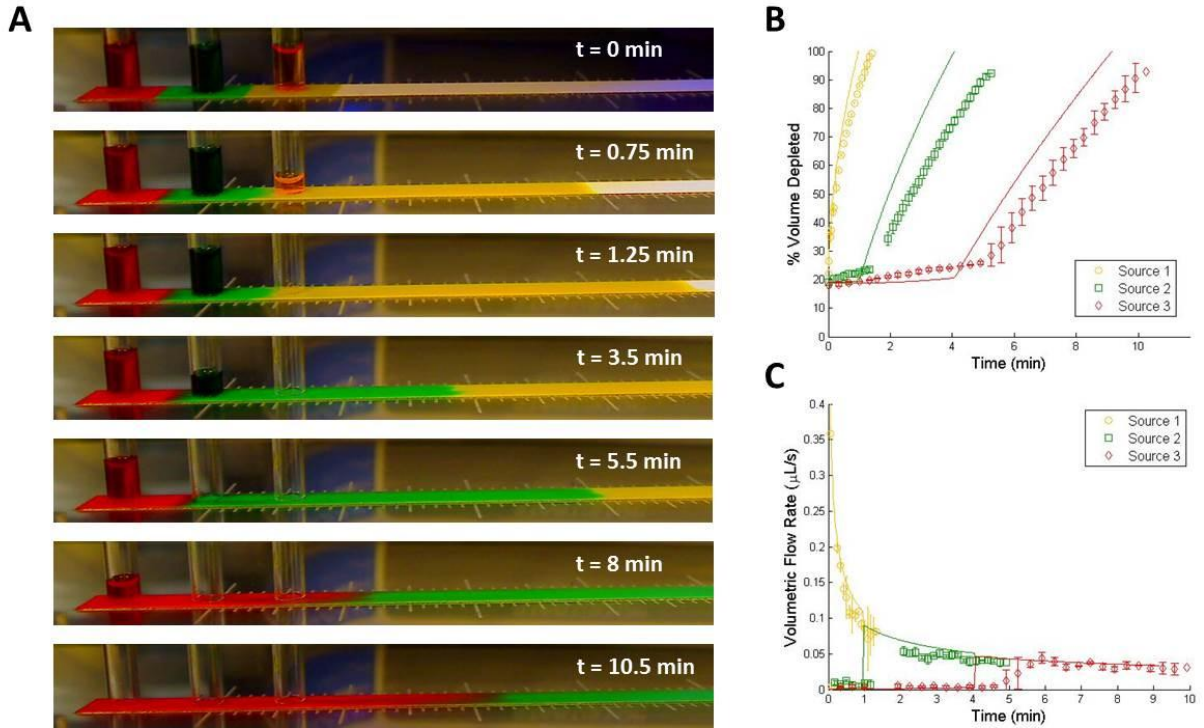
Figure 16. Experimental and model behavior for a Pseudo-1DPN with capillary tube sources. A) Experimental results for Pseudo-1DPN with capillary sources that serve as near ideal sources. Volume-dependent gravitational pressure effects caused slight leakage flow from Sources 2 and 3 but fluid from each source was still delivered in a timed sequence through the strip. Images show the device a few seconds after contact (t = 0 min) and at the moments when each tube was approximately halfway or fully depleted. Ruler markings are spaced 1 mm apart. B) Model and experimental results for percent fluid release over time from all sources in the Pseudo-1DPN. C) Model and experimental results for volumetric flow rate of fluid release from all sources. Similarities between computational and experimental results led us to believe we were capturing the key physical behaviors of the system using this electrical circuit based model. Model results are depicted by a solid line; the averaged experimental results (n=3) are denoted by open faced markers.

Table 5. Time required for each source to be depleted. Drainage times for Sources 2 and 3 were considered only after the previous source was completely drained (n=3).

	Drainage Time [min] (Computational)	Drainage time [min] (Experimental)
Source 1	0.98	1.43 ± 0.09
Source 2	3.1	3.8 ± 0.3
Source 3	5.1	6.6 ± 0.3

From Section 4.2, we predicted that there would be no leakage flow from Sources 2 and 3 if ideal sources were used in a Pseudo-1DPN. In the first stage of the device, only fluid from Source 1 should be released. Once that source was entirely depleted, Source 2 should release its fluid and only after, would Source 3 begin to be depleted. In both our computational and experimental results, we found that there was a small amount of premature fluid release from both Sources 2 and 3. This leakage flow was due to the previously mentioned volume-dependent backpressure exerted by the capillary tubes. However, because the magnitude of the source backpressure was low, the amount of fluid loss attributed to leakage flow was relatively minor in comparison to the total volume delivered from the source (**Table 6**). Mathematically, we calculated that the highest possible leakage flow rate in our system would be 0.003 μL/sec. This rate of release was also negligible in comparison to those of the dominant delivery stages (which computationally, ranged from 0.03 μL/sec to 0.58 μL/sec).

Table 6. *Percent of total volume released by Sources 2 and 3 due to leakage flow (n=3).*

	Volume Released (Computational)	Volume Released (Experimental)
Source 1	-	-
Source 2	0.01%	4% ± 2%
Source 3	0.02%	11% ± 4%

While there were noticeable discrepancies between the computational and experimental results for the system, we found that the computational model was able to predict the general behavior

of a Pseudo-1DPN device with capillary tube sources. However, it is critical to determine the causes of these deviations for more rigorous model validation. Possible causes include:

- Incorporation of inaccurate system parameter values into the model

- The model's inability to account for all consequences of leakage flow

- Optical aberrations from the web camera

- Flow abnormalities from contact between capillary tubes and the wicking membrane

These potential sources of error are further discussed in **APPENDIX VII**.

5.4 Conclusions

In previous work, we chose to use glass fiber pads as fluid sources (*e.g.*, **Figure 5**) based on their use as dry reagent storage media in lateral flow tests, their ability to self-fill to a fixed volume by wicking (potentially eliminating the need for pipetting steps), and our observation that they release nearly all fluid into a nitrocellulose strip. However, here we found that changes in backpressure during release from glass fiber pads required compensation by increasing the spacer length between fluid sources (and thus increasing total device run time).

In contrast, experiments with near ideal fluid sources showed that the Pseudo-1DPN can achieve sequential delivery with little premature fluid release. Similar trends in fluid release and volumetric flow rates between sources were found between the computational and experimental results. Thus, while there were noticeable discrepancies between the computational and experimental results for the system, we found that computational model was able to predict the general behavior of a Pseudo-1DPN device with capillary tube sources.

Chapter 6: HIV Antigen Detection Using a Pseudo-1DPN

In the previous chapter, it was shown that a Pseudo-1DPN device has the potential to perform sequential delivery of reagents through a wicking membrane in a discrete and easily predicted manner. Using the previously defined analytical model, we predict that this is true regardless of the number of sources used and the total volume delivered by each source. In the context of designing a device to perform a multi-step assay, this capability is extremely valuable. Delivery parameters can be easily tuned to fit the requirements of a given assay without having to completely redesign the device to successfully achieve clean sequential delivery. In this chapter, we aim to use a Pseudo-1DPN to perform a multi-step, ELISA based HIV detection assay. This first generation device will not be entirely user-friendly, but will demonstrate the potential this technology has for performing automated, multi-step assays.

6.1 Motivation

In the past few decades, human immunodeficiency virus (HIV) has become a major epidemic throughout the world, becoming one of the greatest threats to human health and development. In 2010, there were an estimated 34 million people living with HIV in the world [71]. While HIV is a serious health issue across the world, it has quickly become a leading killer in the developing world specifically (**Figure 17**). Of the 34 million people living with HIV, approximately 22.9 million of them are located in Sub-Saharan Africa [71]. As a result,

combatting the HIV epidemic has largely focused on reducing the prevalence of the disease in developing countries [72].

While there is currently no cure for HIV, diagnosis of the virus is critical, as it can allow for reduced transmission and earlier initiation of antiretroviral therapy [73,74]. There are currently several commercially available HIV diagnostics that are able to determine, with great sensitivity, if an individual is HIV positive [75]. However, many of these diagnostics are unsuitable for the developing world, where the HIV burden is the greatest [76]. Utilization of these devices in LRS is limited by their inherent cost, the number of laboratories equipped to run the tests, and the underdeveloped transportation infrastructure required to move patient blood samples to equipped laboratories [77]. As a result, populations in LRS are often unaware of their HIV status. In 2009 it was found that over 70% of the HIV infected population in Congo were unaware of their infection [78].
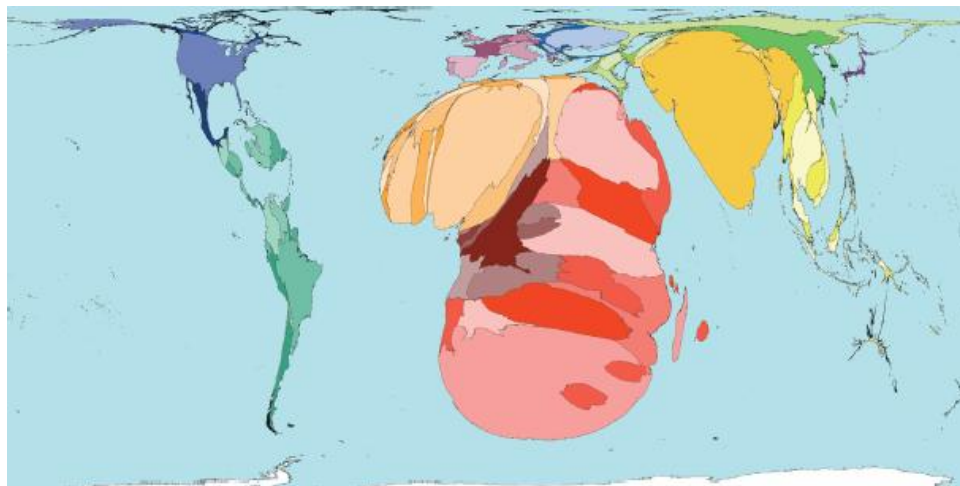
Figure 17. Global distribution of HIV infections © *Copyright Sasi Group (University of Sheffield) and Mark Newman (University of Michigan). World map with territories resized based on the prevalence of HIV demonstrates the high occurrence of HIV in the developing world* [87].

Researchers have worked to increase the availability of HIV diagnostics in LRS by developing tests that are more suited for the conditions in the developing world [8]. One example of such a technology is a rapid, self-performing test that diagnoses HIV infections by detecting the presence of HIV antibodies in a patient's blood [76]. This form of diagnostic satisfies the restrictions previously mentioned and is heavily utilized in LRS. However, this diagnostic tool is limited in its ability detect acute infections, when an individual is HIV antigen positive but HIV antibody negative [76]. There exists, on average, a 22 day window period between HIV infection and a detectable HIV antibody titer (**Figure 18**). Therefore, individuals who use an HIV antibody diagnostic test soon after infection may receive a false negative result [79].

In order to reduce this window period, a combination HIV antigen/antibody assay has been developed [80]. HIV p24 antigen can reach detectable limits in the bloodstream within approximately two weeks of infections. Thus, in comparison to an antibody test, these
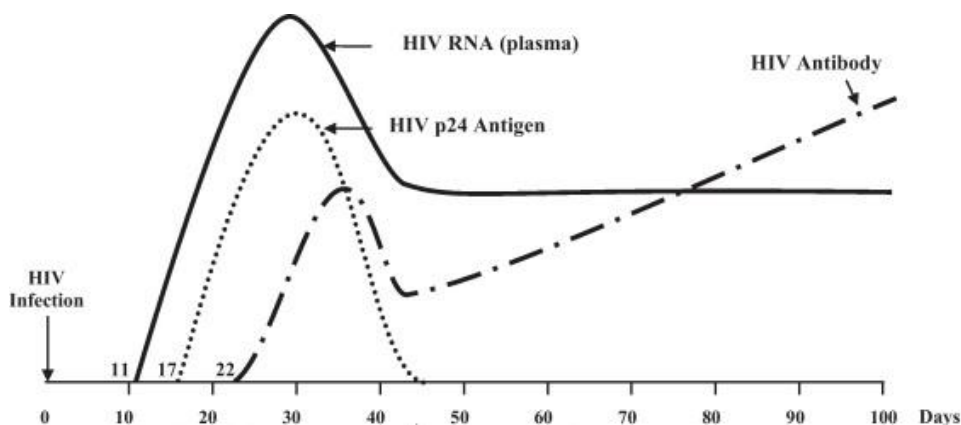
Figure 18. Window of detection of various HIV biomarkers [figure source: Patel, P. et al. Rapid HIV screening: missed opportunities for HIV diagnosis and prevention. Journal of clinical virology 54, 42-7 (2012)]. HIV p24 antigens are formed at an earlier stage of infection than HIV antibodies. A p24 antigen diagnostic would have the potential to reduce the false negative detection window by approximately one week [79].

combination assays (which are commonly performed using an ELISA) have been able to diagnosis people at an earlier stage of infection [76].

Early detection of HIV infections in LRS could lend itself to applications that span the clinical, public health, and research sectors of HIV [75]. People with acute HIV infections are often more infectious than those in a later infection state due to their higher HIV viral load [74]. As a result, they generally contribute disproportionately to ongoing HIV transmission. In addition, research suggests that early initiation of antiretroviral therapy (ART) can potentially improve health outcomes for acutely infected individuals [81]. A sensitive antigen detection assay could also be of great use for diagnosing HIV in infants born to HIV-infected women. Maternal anti-HIV antibodies can be found in the infant's blood for the first fifteen to eighteen months of life, making standard HIV antibody tests an ineffective diagnostic tool [82]. Early HIV detection is also essential for screening blood and plasma to ensure blood supplies remain safe and uninfected [83]. Finally, a great priority in current HIV research is to better understand the early immune response of HIV [84]. Being able to identify acutely infected individuals could be useful for developing improved biomedical prevention measures, such as HIV vaccines and microbicides [85].

Researchers have used technologies like the conventional lateral flow test strip to create an HIV antibody/antigen detection system that uses only a single chemical delivery step [85]. However, simplification of these assays has shown to cause analytical sensitivity to no longer reach a relevant antigen limit of detection (15 – 50 pg/mL) [86]. Thus, providing a way to incorporate

the sensitive, multi-step ELISA based assay into a technology that is actually suitable for LRS may lead to the development of a clinically valuable HIV diagnostic.

The demonstrated capabilities of a Pseudo-1DPN suggest its utility in accomplishing such a goal. Its ability to automatically perform multiple reagent delivery steps in a well predicted manner makes it a platform that can potentially achieve desired analytically sensitivity levels, while still meeting the demands of a device relevant in LRS.

6.2 Materials and Methods

HIV p24 antigen detection was performed using three different methods: conventional ELISA, a manual paper-based 'dipstick' test, and an automated Pseudo-1DPN.

Materials. The following commercially available ELISA reagents were used: monoclonal HIV-1 p24 antibody (Bio-Rad, Redmond, WA), biotinylated polyclonal antibodies to HIV p24 antigen (Bio-Rad, Redmond, WA), and horse radish peroxidase (HRP) – conjugated streptavidin (Invitrogen, Grand Island, NY). Bio-Rad reagents were from their commercially available HIV Ag/Ab Combo EIA kit and were kindly donated by the company. Recombinant p24 antigen (Abcam, Cambridge, MA) was used to stand-in as a patient sample.

The monoclonal p24 antibody served as a capture antibody, while the biotinylated antibody was used to label any bound antigen. HRP-streptavidin was used to bind biotin-labeled complexes and diaminobenzidine (DAB) or tetramethylbenzidine (TMB) were used as the detection system, as they can be oxidized to create a visual signal.
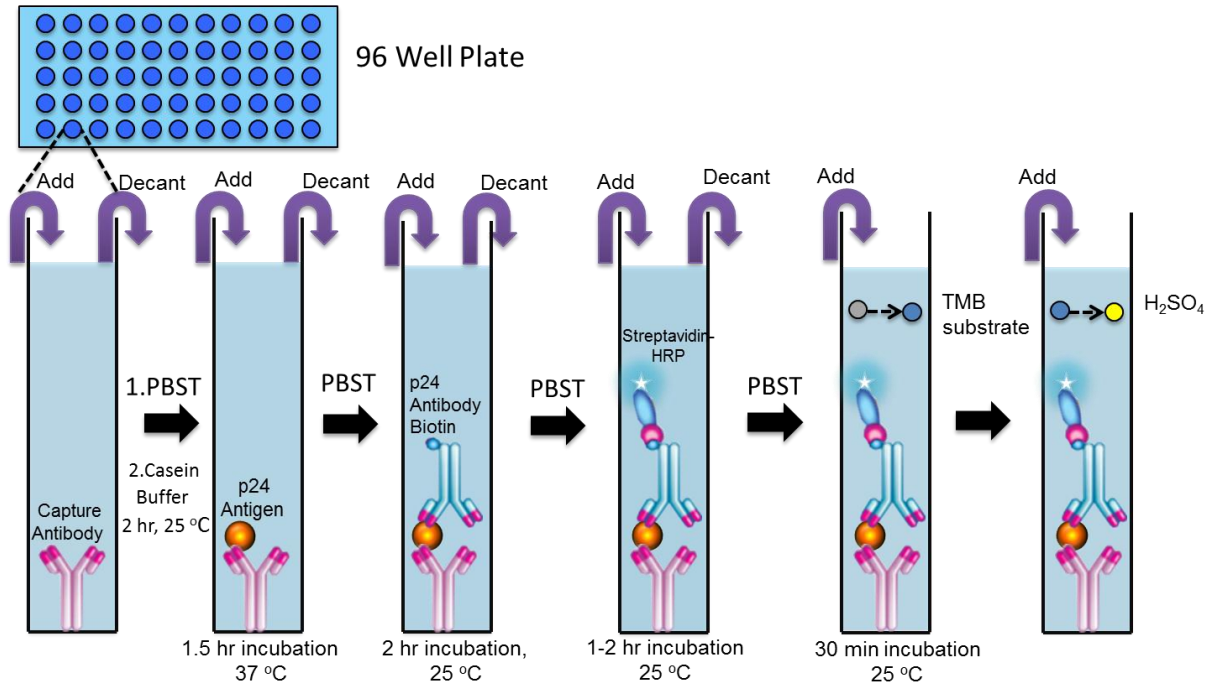
Figure 19. Schematic of HIV p24 antigen ELISA assay [figure source: Nuttada Panpridist, Lutz Lab]. *The assay requires at least six hours to run (not including the overnight capture antibody incubation period), incubations at several different, well-controlled temperatures, and the use of a plate reader. These conditions make it not well suited for use in LRS.*

ELISA Methods. An ELISA for p24 antigen was designed for our given set of reagents using a sample protocol provided by Abcam (**Figure 19**). 50 μL capture antibody diluted in phosphate buffer saline (PBS) solution (10 μg/mL) was incubated in a polystyrene 96 well plate overnight at 4°C. Subsequently, all remaining well surfaces were blocked using a blocking buffer of 300 μL 0.05% casein buffer in PBS with 0.05% Tween-20 to reduce non-specific adsorption using. Wells were covered and incubated for two hours at room temperature. 100 μL of antigen sample diluted in PBS was then incubated for 90 minutes at 37°C. The well was subsequently incubated with 100 μL biotinylated antibody diluted in blocking buffer (200 ng/mL) for two hours at room temperature, followed by 100 μL HRP-streptavidin (200 ng/mL, blocking buffer) for one to two hours at room temperature. 100 μL TMB was introduced to the well for 15 to 30 minutes at

room temperature. The reaction was halted by adding 100 µL 2 M H₂SO₄ to the TMB solution. Absorbance of the well solution was measured at a wavelength of 450 nm using a plate reader (Infinite 200 Pro; Tecan, Männedorf, Switzerland). Before each new reagent added to the well (except H₂SO₄), the previously incubated solution was removed and the well was washed two to four times with 300 µL PBS with 0.1% Tween-20 (PBST).

Manual 'Dipstick' Methods. An initial p24 antigen paper-based "dipstick" assay was designed in consideration of a successful protocol previously developed by the Yager Group for detection of a malarial antigen [55]. 2 µL capture antibody was spotted by hand at a concentration of 0.5 mg/mL (diluted in PBS) onto a 3 mm x 24 mm nitrocellulose membrane strip. All assay solutions were contained in a polystyrene 96 well plate. The strip was placed vertically in a well, allowing the reagent of interest to wick through the membrane and pass over the capture area (**Figure 20**). The membrane was then (manually) moved into a well that contained the subsequent assay reagent to continue the assay. Two 25 µL PBST washes were performed between each assay step in the same way. Strips were moved to the subsequent well after a specified time. The assay reagent order was as follows: 25 µL p24 antigen (diluted in FBS, Δt = 4 minutes), 25 µL biotinylated antibody (diluted to 10 µg/mL in PBST, Δt = 4 minutes), 25 µL HRP-streptavidin (diluted to 10 µg/mL in PBST, Δt = 4 minutes), and 40 µL DAB (0.25 mg/mL DAB, 0.1% sodium percarbonate, Δt = 6 minutes).
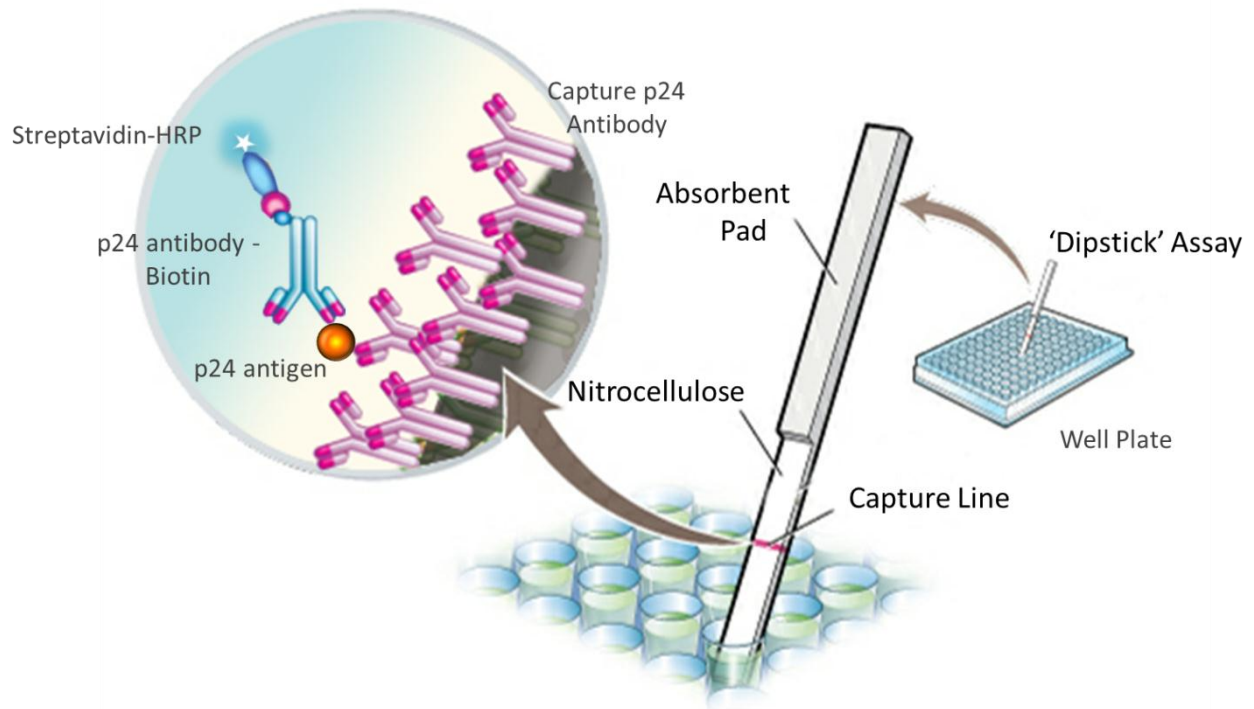
Figure 20. Schematic of HIV p24 antigen paper-based "dipstick" assay [figure source: Nuttada Panpridist, Lutz Lab]. The assay requires less than one hour to run (not including the overnight capture antibody incubation period) and the use of a scanner; fluid delivery time is controlled manually. This assay form is still non-ideal for a POC test; however, it is a useful testing platform to demonstrate assay functionality.

Assay signal was recorded using a scanner (Epson Perfection V700) and quantified using a MATLAB program developed by Nuttada Panpradist, a research technician in the Lutz group. Briefly, a box is positioned around the capture spot and the optical density (OD) (95th percentile) of the spot is determined. The background signal for each spot (the OD of a boxed area underneath each spot) is subtracted from the spot OD to determine the overall signal achieved.

6.3 HIV p24 Antigen ELISA

There was a clear dose-response between HIV p24 antigen concentration and OD signal (**Figure 21**). Visual observation of a graph of signal versus antigen concentration showed that signal noticeably increased once reaching an antigen concentration of approximately 75 pg/mL. We

estimated the limit of detection (LOD), or the lowest amount of antigen distinguishable from a blank sample, using the equation,

$$OD_{LOD} = OD_{Blank} + 3SD_{Blank} \tag{22}$$

Summing the signal and standard deviation (SD) associated with a blank sample gave us the lowest OD value that corresponds to a positive sample. Using five blank samples, the LOD for this ELISA assay was determined to be between 40 pg/mL and 50 pg/mL. This range closely matched the analytical sensitivity claimed by Bio-Rad (~25 pg/mL), demonstrating that the ELISA reagents were functional and compatible with the separately purchased recombinant p24 antigen.
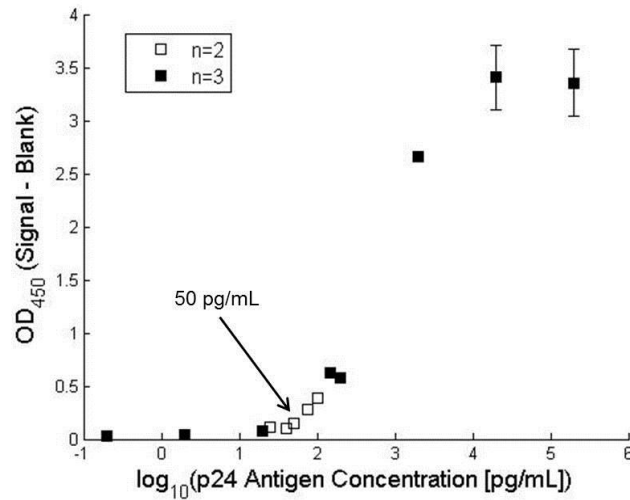
Figure 21. HIV p24 antigen ELISA results. The ELISA shows a clear dose-response between signal and antigen concentration. We calculated a LOD of between 40 − 50 pg/mL antigen, which is comparable to that cited by Bio-Rad. Filled in markers points were the average of n=3 trials. Open faced marker points were the average of n=2 trials. Standard deviations were provided for only the points with n=3.

6.4 Manual HIV p24 Antigen "Dipstick" Paper-Based Assay

The first goal towards creating a POC HIV antigen diagnostic was to ensure that the p24 antigen ELISA could be translated into a paper-based assay with a reasonable analytical sensitivity level. In first attempts to convert this assay, a nitrocellulose strip spotted with capture antibody was simply dipped into a well that contained the reagent of interest. Fluid delivery time was controlled by manually moving the strip to the subsequent well once the given step is complete. While this format is non-ideal for a POC device, its basic design makes it a useful platform to test assay functionality.

As a note, FBS was used as a diluent for the antigen because, 1) in comparison to a simple buffer solvent, the proteins present in the sample provide a more realistic representation of a blood sample that would be used in a true assay, and 2) the large proteins non-specifically attach to free regions of the nitrocellulose membrane due to electrostatic effects, minimizing the amount of reagent lost to nonspecific adsorption (known as real time blocking).

Initial results for this assay showed a noticeable dose-response between antigen concentration and signal OD (**Figure 22A,** 'FBS Block'). While there was a visually observable signal for the blank sample, we saw that the signal intensity increased with higher antigen concentrations. This higher signal was most obvious at antigen concentrations of 2 ng/mL and 20 ng/mL. For this first generation paper-based assay, we found a LOD of between 500 pg/mL and 2 ng/mL antigen concentration. While this LOD was significantly higher than that of the conventional ELISA and what was needed to be clinically relevant, it was clear that these ELISA reagents

could be used to create a functioning paper-based assay. Additionally, this lateral flow based assay required smaller reagent volumes and significantly less time to perform. Total run time was approximately 46 minutes, which was highly improved from the minimum six hours required to perform a conventional ELISA.

Incorporation of this assay into a Pseudo-1DPN may require several modifications to be made, as the device platform is significantly altered. In the 'dipstick' assay, the membrane appears to sufficiently block non-specific adsorption of reagents when only the first delivered reagent (antigen) is diluted in FBS, as the FBS wicks through all exposed areas of the membrane. However, in the case of a Pseudo-1DPN, each fluid source initially wets out a naïve, unblocked
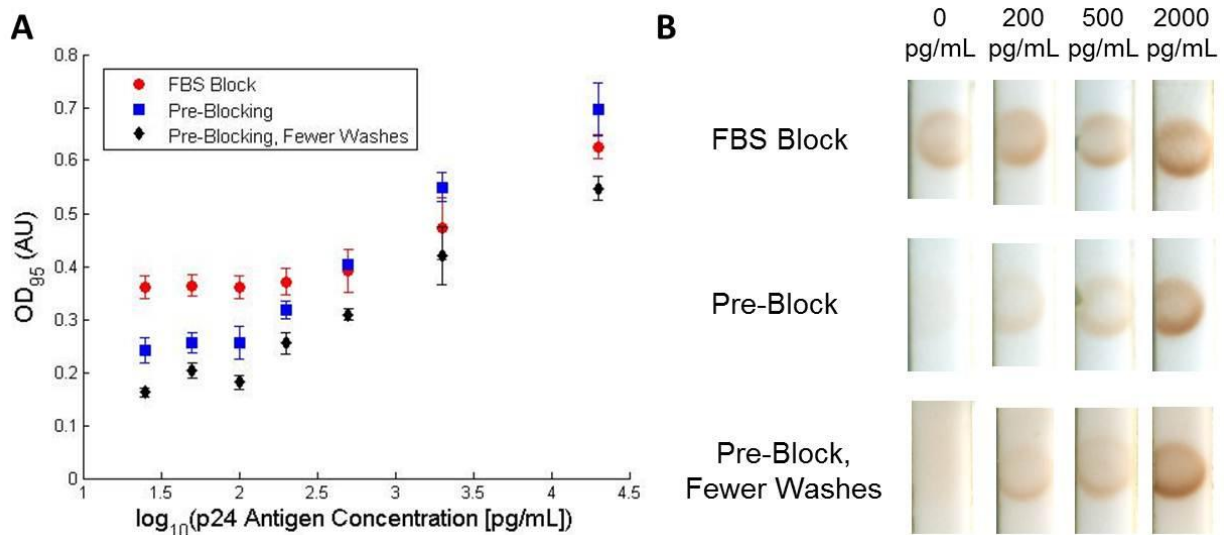
Figure 22. Manual 'dipstick' p24 assay results. A)Signal intensity is shown as a function of p24 antigen concentration. There is a clear dose response, demonstrating the ELISA based reagents can be used in a paper-based assay. Results from three different 'dipstick' protocols are reported: all wash steps and only a FBS real-time block, all wash steps and a pre-blocked membrane, reduced wash steps and a pre-blocked membrane (n=3). B) Images of the capturea area on the nitrocellulose membrane given all three protocols at a variety of different antigen concentrations. Signal from the negative control (0 pg/mL) is dramatically reduced by pre-blocking. Visually, the LOD appears to decrease with pre-blocking. Strip width was 3 mm.

area of the membrane. While a large portion of the membrane would be blocked by the FBS, membrane regions upstream of the antigen fluid source would be unblocked, and it is likely that a large amount of reagent would be lost on the membrane before reaching the capture line. We can potentially avoid this issue by pre-blocking all areas of the strip before its use. This can be done by incubating the strips in a 1X HIV Western Blot Blocking (Bio-Rad, Redmond, WA) solution at room temperature for two hours (after the capture antibody has been spotted and dried overnight), and subsequently, drying them in a desiccator.

Additionally, limiting the number of required steps would be useful for minimizing assay complexity and device run time. This would most easily be achieved by eliminating some PBST washes, which make up the majority of delivery steps. Ideally, we would eliminate all PBST washes. However, this could potentially cause unwanted interactions and binding events to occur between reagents. For example, in a Pseudo-1DPN, fluids from neighboring sources can be in contact for an extended period time. In the specific case of HRP=labeled streptavidin and DAB, interactions between the reagents can lead to premature precipitate formation that impedes flow to downstream regions of the membrane. A wash could be included between these two reagent delivery steps to eliminate these detrimental premature interactions. Also, the final fluid delivered in a Pseudo-1DPN does not travel as far along the membrane as more downstream reagents do; a significant percentage of the fluid released might not even reach the capture line. A PBST wash could be used to push the otherwise lost final reagent over the capture area.

Thus, while it may be possible to eliminate several wash steps from the initial assay protocol, we predict that washes before and after the DAB delivery step may actually be useful for maintaining a successful assay. Taking this into account, we revise our initial 'dipstick' assay protocol to remove all wash steps between the first three reagent delivery steps, while still including a 25 µL PBST before and after DAB delivery.

Experimentally, these two alterations (pre-blocking and elimination of specific wash steps) were both shown to actually improve overall assay performance (**Figure 22A**). Pre-blocking the strips significantly reduced the signal of a blank sample and improved the LOD (OD_{LOD} = 0.32 AU) to a concentration of approximately 200 pg/mL (0.32 AU ± 0.02). Pre-blocking the strip and eliminating wash steps between the first three reagent delivery steps was shown to further reduce the signal of blank sample. This decrease in signal was attributed to the higher background signal of the strip (in comparison to when all washes were included) (**Figure 22B**). The LOD achieved by this protocol was less than 200 pg/mL antigen (0.26 AU ± 0.02 AU, OD_{LOD} = 0.21). This detection limit was approaching the range of clinical relevance (<50 pg/mL) and the sensitivity limit of the conventional ELISA (~25 pg/mL). However, in contrast to a conventional ELISA test, assay run time following this final protocol was reduced to only 26 minutes.

6.5 Automated HIV p24 Antigen Diagnostic Device

A Pseudo-1DPN can theoretically be used to perform sequential delivery, regardless of source number and fluid volume. Thus, we can increase the number of sources used in previously demonstrated devices to fulfill the needs of the manual 'dipstick' assay.

We chose to use capillary tube sources in this device because they are small in size but are still able to contain the desired fluid volumes. The amount of leakage flow that occurs with these sources appears to be relatively low. However, leakage flow is dependent on the pressure differential between sources and, by relation, the volume contained by each capillary source. To reduce leakage, differences in fluid volumes between sources should be minimized. In contrast to the 25 µL of fluid delivered in nearly all steps of the 'dipstick' assay, 40 µL DAB was used. In a Pseudo-1DPN, this deviation in fluid volume would lead to increased leakage flow. Rather than limiting DAB delivery volume to 25 µL, we split delivery into two sequential 25 µL steps, allowing total DAB delivery volume to be 50 µL without increasing leakage flow.

Additionally, we previously found that the rate of delivery of the first fluid in a Pseudo-1DPN is significantly greater than that of later fluids. In an assay, this can lead to insufficient interaction time between capture line and analyte. We can improve interaction time by increasing the space between analyte source and the capture line; the flow rate of the analyte will have decreased by the time it reaches the capture line. However, this would cause device operation time to drastically increase, as the flow rate of subsequent delivery steps would also decrease. For this first generation automated p24 assay, we accounted for this fast flow rate by increasing the volume of sample delivered to 50 µL (again, as two sequential 25 µL delivery steps). Finally, to ensure all DAB is wicked past the previous sources and through the capture line, we increased the number of PBST washes that follow DAB delivery to three sequential 25 µL steps (75 µL PBST wash in total).

With these assay modifications, the Pseudo-1DPN must now perform sequential delivery with ten sources, each containing 25 µL. This sounds like a daunting task, but one of the major advantages of using a Pseudo-1DPn design (in comparison to a 2DPN) is that scaling it up to accomplish this goal requires little effort. The wicking membrane strip must be lengthened to accommodate the additional area required to contain such a large number of sources and the capillary tube must be refabricated to hold ten capillary tubes a set distance apart. Apart from these minor changes, the design decisions previously made for the three-stage Pseudo-1DPN should still be relevant to this more complex device. We maintained a nitrocellulose membrane width of 4 mm and a source spacing distance of 4.25 mm. A total fluid volume of 250 µL was delivered in the assay; containing this volume of fluid would require an extremely long nitrocellulose strip and would cause upstream delivery stages to occur at very low flow rates. Therefore, we included a thick cellulose absorbent pad (GR320; Ahlstrom, Helsinki, Finland) after the capture line to reduce overall operation time. This alteration should have no effect on the key physical behavior of the system. The rate of fluid delivery over the capture line is likely to change, as the capillary pressure of an absorbent pad is not the same as that of the nitrocellulose membrane. However, the presence of an absorbent pad should not affect the pressure differential between sources and thus, the success of sequential delivery. Sequential delivery in this more complex Pseudo-1DPN was demonstrated using colored fluids in **APPENDIX VIII.**

Results. A functional and automated p24 antigen assay was achieved using this Pseudo-1DPN device. We saw a visually distinguishable difference in signal intensity between the blank sample and samples with approximately 100 pg/mL – 200 pg/mL antigen present (**Figure 23**). A blank sample produced a slightly visible signal, which was similar to that of the pre-blocked, reduced wash manual 'dipstick' test. We were unable to perform LOD analysis for this device due to an insufficient number of data sets; however, we saw that there was a clear dose response between antigen concentration and OD. The data point for 200 pg/mL antigen was not shown on the dose-response curve because the OD value generated for this device did not seem to match what
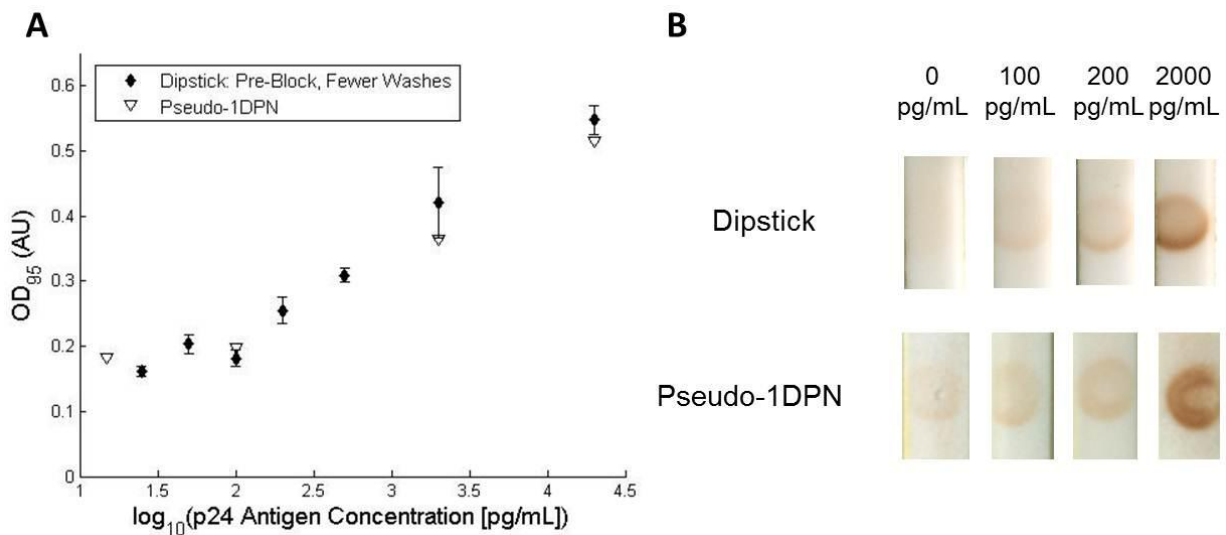
Figure 23. Pseudo-1DPN p24 assay results in comparison to the related 'dipstick' test. A) Signal intensity is shown as a function of p24 antigen concentration. The results of the manual 'dipstick' test with pre-blocking and reduced wash steps is shown again for comparison. The signal intensitys achieved by the Pseudo-1DPN appeared to match relatively well with the manual test. B) Images of the capture area given the same two protocols (maual with pre-blocking and fewer wash steps, Pseudo-1DPN) at a variety of antigen concentrations. Visually, the LOD of the Pseudo-1DPN appeared to be approximately 200 pg/mL. Strip width for the manual assay was 3 mm. Strip width for the Pseudo-1DPN was 4 mm.

was visually observed (OD_{blank} = 0.18, $OD_{100pg/mL}$ = 0.20, $OD_{200pg/mL}$ = 0.19); we believe there was some artifact on the strip that caused an inaccurate representation of the signal. Total device operation time was 71 min ± 6 min.

6.6 Conclusions

We were able to convert an ELISA based HIV p24 antigen assay into an automated, paper-based diagnostic with a significantly reduced operation time. Translating the manual 'dipstick' assay design into an automated device was a relatively simple process due to our understanding of the fluidic behavior of the system. Furthermore, the robustness of the Pseudo-1DPN platform allows great flexibility in altering the assay protocol. We believe the sensitivity of our Pseudo-1DPN HIV assay is approximately 200 pg/mL, making it approach clinical relevancy.

Chapter 7: Conclusions and Future Directions

7.1 Conclusions

The lateral flow test is an ingenious device that performs basic immunoassays in a rapid and easy-to-use format. Paper networks use the same set of materials but reconfigure them to automatically carry out timing for multi-step processes. The behavior of both devices depends on the connectivity of multiple materials and their wicking properties. Here, we explored basic principles of wicking in simple devices and paper networks through use of electrical circuit models. We identified key design principles in a previously-developed sequential delivery device (2DPN) and described an alternative linear paper network (Pseudo-1DPN) that can provide remarkably clean sequential delivery in a very simple device. We showed that materials used as fluid sources can affect both the rate of fluid delivery into a strip and the fraction of fluid volume released, and these fluid release properties are especially important for programming sequential delivery in paper networks. Finally, a Psuedo-1DPN was used to perform a multi-step HIV p24 antigen assay, demonstrating the relevancy of this platform as an automated diagnostic. The analysis provides a framework for more rational design and material selection for paper networks and other capillary-driven diagnostic devices.

7.2 Future directions

Model validation. More stringent validation of the electrical circuit model could greatly increase the application of this computational tool. In this thesis, we used modeling to identify key

behaviors within a device system. Ideally, this model could be used to quantitatively predict the fluidic behavior in a device. This could provide extremely useful insight for assay optimization, as critical design parameters, such as reagent interaction times, could be taken into account when designing a device.

Initial results showed that there are currently some discrepancies between our computational model and the experimental results. This is likely due to the inclusion of an inaccurate membrane parameter value or incorrect assumption during model implementation. A simple parameter fit can be performed on the experimental data to determine what membrane parameter values would be required to accurately describe the system. If these values are found to be within reason (based on literature values or experimentally generated values), it is likely that the deviations between results were caused by an incorrect parameter value. If this is not the case, it is possible that one of our assumptions is not true. Factors that were previously regarded as being insignificant, such as leakage flow, would need to be reconsidered and potentially be accounted for in the model.

If we are able to eliminate discrepancies between the experimental and computational results for a given system, we must then explore the behavior of devices with several altered design parameters (such as fluid volume, number of sources, device geometry, and source material). This will identify limitations of the model or provide additional validation that the model can be used to predict device behavior.

HIV p24 antigen assay. Using a Pseudo-1DPN, we developed a multi-step p24 antigen assay that was automated and was believed to have an analytical sensitivity level that approaches

clinical relevance. While this is a relatively significant accomplishment and a critical first step in diagnostic development, practically speaking, the current device is unusable in a real world setting. Assay set-up is time consuming and demanding, operation time is longer than desired, and the assay still does not have a relevant LOD. In our ideal diagnostic device, a user would simply add sample and buffer to specified regions of the device and then pull a tab to initiate delivery. All assay reagents would be pre-dried within the device and all elements of the Pseudo-1DPN (except the read-out signal) would be concealed.

The Fu/Lutz./Yager Group has previously used glass fiber pads to store dried reagents. However, since we found that glass fiber sources are not very useful in the context of a Pseudo-1DPN, we must either find a way to dry reagents in capillary tubes, or identify an alternative pad-like source material that has the desired fluid release properties. Additionally, we must develop a mechanical method for "activating" delivery in the device. Activation will consist of two different steps: 1) sample/buffer delivery to the sources, and 2) fluid release from the sources into the membrane. Both of these transfers must be highly reproducible and robust.

Finally, for this device to have clinical relevance, we must improve its operation time and LOD. Operation time could potentially be reduced by limiting fluid volumes and/or delivery steps, increasing the width of the membrane, decreasing spacing between sources, or using a nitrocellulose membrane with a higher capillary pressure. LOD could potentially be improved by increasing reagent concentrations and/or increasing interaction times between reagents and the capture line. Ideally, we could calculate the flow rates at which each reagent maximally binds to

the capture line and then use the validated computational model to design a device that satisfies these criteria.

REFERENCES

[1]   C. P. Price, "Clinical review Point of care testing," 1285–1288 (2001).

[2]   S. K. Sia and L. J. Kricka, "Microfluidics and point-of-care testing.," *Lab on a chip* **8**(12), 1982–1983 (2008) [doi:10.1039/b817915h].

[3]   S. S. Ehrmeyer and R. H. Laessig, "Point-of-care testing, medical error, and patient safety: a 2007 assessment.," *Clinical chemistry and laboratory medicine : CCLM / FESCC* **45**(6), 766–773 (2007) [doi:10.1515/CCLM.2007.164].

[4]   F. a Gomez, "The future of microfluidic point-of-care diagnostic devices.," *Bioanalysis* **5**(1), 1–3 (2013) [doi:10.4155/bio.12.307].

[5]   P. Yager, G. J. Domingo, and J. Gerdes, "Point-of-care diagnostics for global health.," *Annual review of biomedical engineering* **10**, 107–144 (2008) [doi:10.1146/annurev.bioeng.10.061807.160524].

[6]   R. L. Cook, L. Østergaard, S. L. Hillier, P. J. Murray, C.-C. H. Chang, D. M. Comer, and R. B. Ness, "Home screening for sexually transmitted diseases in high-risk young women: randomised controlled trial.," *Sexually transmitted infections* **83**(4), 286–291 (2007) [doi:10.1136/sti.2006.023762].

[7]   R. P. Walensky and A. D. Paltiel, "Annals of Internal Medicine Perspective Rapid HIV Testing at Home : Does It Solve a Problem or Create One ? AT" (2013).

[8]   P. Yager, T. Edwards, E. Fu, K. Helton, K. Nelson, M. R. Tam, and B. H. Weigl, "Microfluidic diagnostic technologies for global public health.," *Nature* **442**(7101), 412–418 (2006) [doi:10.1038/nature05064].

[9]   P. von Lode, "Point-of-care immunotesting: approaching the analytical performance of central laboratory methods.," *Clinical biochemistry* **38**(7), 591–606 (2005) [doi:10.1016/j.clinbiochem.2005.03.008].

[10] R. E. Black, S. S. Morris, and J. Bryce, "Child survival I Where and why are 10 million children dying every year ?," 2226–2234 (2003).

[11] D. M. Morens, G. K. Folkers, and A. S. Fauci, "The challenge of emerging and re-emerging infectious diseases.," *Nature* **430**(6996), 242–249 (2004) [doi:10.1038/nature02759].

[12] a S. Fauci, "Infectious diseases: considerations for the 21st century.," *Clinical infectious diseases : an official publication of the Infectious Diseases Society of America* **32**(5), 675–685 (2001) [doi:10.1086/319235].

[13] M. Dwortzan, "Klapperich Advances Point-of-Care Infection Disease Diagnostics," in *BU Biomedical Engineering* (2013).

[14] S. Sazawal, R. E. Black, P. Case, and M. Trials, "Review Effect of pneumonia case management on mortality in neonates , infants , and preschool children : a meta-analysis of community-based," 547–556.

[15] R. W. Peeling, K. K. Holmes, D. Mabey, and a Ronald, "Rapid tests for sexually transmitted infections (STIs): the way forward.," *Sexually transmitted infections* **82 Suppl 5**, v1–6 (2006) [doi:10.1136/sti.2006.024265].

[16] Y.-H. Hsieh, C. a Gaydos, M. T. Hogan, O. M. Uy, J. Jackman, M. Jett-Goheen, A. Albertie, D. T. Dangerfield, C. R. Neustadt, et al., "What qualities are most important to making a point of care test desirable for clinicians and others offering sexually transmitted infection testing?," *PloS one* **6**(4), e19263 (2011) [doi:10.1371/journal.pone.0019263].

[17] R. W. Peeling, D. Mabey, A. Herring, and E. W. Hook, "Why do we need quality-assured diagnostic tests for sexually transmitted infections?," *Nature reviews. Microbiology* **4**(12 Suppl), S7–19 (2006) [doi:10.1038/nrmicro1569].

[18] S. kitpakdeebodin J Thinkhamrop, P lumbiganon, "Loss to follow-up of patients with abnormal Pap smear: magnitude and reasons," *J Med Assoc Thai* **81**, 862–865 (1998).

[19]   L. B. Ochola, P. Vounatsou, T. Smith, M. L. H. Mabaso, and C. R. J. C. Newton, "The reliability of diagnostic techniques in the diagnosis and management of malaria in the absence of a gold standard.," *The Lancet infectious diseases* **6**(9), 582–588 (2006) [doi:10.1016/S1473-3099(06)70579-5].

[20]   L. E. a Kivihya-Ndugga, M. R. a van Cleeff, W. a Githui, L. W. Nganga, D. K. Kibuga, J. a Odhiambo, and P. R. Klatser, "A comprehensive comparison of Ziehl-Neelsen and fluorescence microscopy for the diagnosis of tuberculosis in a resource-poor urban setting.," *The international journal of tuberculosis and lung disease : the official journal of the International Union against Tuberculosis and Lung Disease* **7**(12), 1163–1171 (2003).

[21]   S. Mavandadi, S. Dimitrov, S. Feng, F. Yu, U. Sikora, O. Yaglidere, S. Padmanabhan, K. Nielsen, and A. Ozcan, "Distributed medical image analysis and diagnosis through crowd-sourced games: a malaria case study.," *PloS one* **7**(5), e37245 (2012) [doi:10.1371/journal.pone.0037245].

[22]   F. F. Mandy, "Twenty-Five Years of Clinical Flow Cytometry : AIDS Accelerated Global Instrument Distribution," *Lancet, The* **56**, 55–56 (2004) [doi:10.1002/cyto.a.10102].

[23]   C. S. Ferreira-Facio, C. Milito, V. Botafogo, M. Fontana, L. S. Thiago, E. Oliveira, A. S. da Rocha-Filho, F. Werneck, D. N. Forny, et al., "Contribution of multiparameter flow cytometry immunophenotyping to the diagnostic screening and classification of pediatric cancer.," *PloS one* **8**(3), e55534 (2013) [doi:10.1371/journal.pone.0055534].

[24]   S. Takeda, N. Hinata, H. Kanda, A. Suzuki, T. Shioyama, Y. Ishikawa, T. Ymaguch, and Y. Kato, "Flow cytometry as a diagnostic method for colorectal cancer," *Cell*, 1004–1007 (2012).

[25]   J. B. Oliveira and T. A. Fleisher, "Molecular- and Flow Cytometry-based Diagnosis of Primary Immunodeficiency Disorders," *Allergy*, 460–467 (2010) [doi:10.1007/s11882-010-0137-8].

[26]   B. I. Fluid, "Correlation Between Cell Samples from Biopsy and Bladder Irrigation Fluid" (1980).

[27]   S. C. Hur, H. T. K. Tse, and D. Di Carlo, "Sheathless inertial cell ordering for extreme throughput flow cytometry.," *Lab on a chip* **10**(3), 274–280 (2010) [doi:10.1039/b919495a].

[28]   A. J. Mach, J. H. Kim, A. Arshi, S. C. Hur, and D. Di Carlo, "Automated cellular sample preparation using a Centrifuge-on-a-Chip.," *Lab on a chip* **11**(17), 2827–2834 (2011) [doi:10.1039/c1lc20330d].

[29]   A. J. Mach and D. Di Carlo, "Continuous scalable blood filtration device using inertial microfluidics.," *Biotechnology and bioengineering* **107**(2), 302–311 (2010) [doi:10.1002/bit.22833].

[30]   D. R. Gossett, W. M. Weaver, A. J. Mach, S. C. Hur, H. T. K. Tse, W. Lee, H. Amini, and D. Di Carlo, "Label-free cell separation and sorting in microfluidic systems.," *Analytical and bioanalytical chemistry* **397**(8), 3249–3267 (2010) [doi:10.1007/s00216-010-3721-9].

[31]   S. C. Hur, N. K. Henderson-MacLennan, E. R. B. McCabe, and D. Di Carlo, "Deformability-based cell classification and enrichment using inertial microfluidics.," *Lab on a chip* **11**(5), 912–920 (2011) [doi:10.1039/c0lc00595a].

[32]   G. S. Fiorini and D. T. Chiu, "Disposable microfluidic devices: fabrication, function, and application.," *BioTechniques* **38**(3), 429–446 (2005).

[33]   T. P. Burg, M. Godin, S. M. Knudsen, W. Shen, G. Carlson, J. S. Foster, K. Babcock, and S. R. Manalis, "Weighing of biomolecules, single cells and single nanoparticles in fluid.," *Nature* **446**(7139), 1066–1069 (2007) [doi:10.1038/nature05741].

[34]   A. Hatch, A. E. Kamholz, G. Holman, P. Yager, and K. F. Böhringer, "A Ferrofluidic Magnetic Micropump," 215–221 (2001).

[35] A. Hatch, A. E. Kamholz, K. R. Hawkins, M. S. Munson, E. A. Schilling, B. H. Weigl, and P. Yager, "R ESEARCH A RTICLE A rapid diffusion immunoassay in a T-sensor," *Group* **19**(May), 461–465 (2001).

[36] A. W. Martinez, S. T. Phillips, G. M. Whitesides, and E. Carrilho, "Diagnostics for the developing world: microfluidic paper-based analytical devices.," *Analytical chemistry* **82**(1), 3–10 (2010) [doi:10.1021/ac9013989].

[37] B. Ngom, Y. Guo, X. Wang, and D. Bi, "Development and application of lateral flow test strip technology for detection of infectious agents and chemical contaminants: a review.," *Analytical and bioanalytical chemistry* **397**(3), 1113–1135 (2010) [doi:10.1007/s00216-010-3661-4].

[38] X. Li, D. R. Ballerini, and W. Shen, "A perspective on paper-based microfluidics: Current status and future trends.," *Biomicrofluidics* **6**(1), 11301–1130113 (2012) [doi:10.1063/1.3687398].

[39] B. Weigl, G. Domingo, P. Labarre, and J. Gerlach, "Towards non- and minimally instrumented, microfluidics-based diagnostic devices.," *Lab on a chip* **8**(12), 1999–2014 (2008) [doi:10.1039/b811314a].

[40] D. R. Ballerini, X. Li, and W. Shen, "Patterned paper and alternative materials as substrates for low-cost microfluidic diagnostics," *Microfluidics and Nanofluidics* **13**(5), 769–787 (2012) [doi:10.1007/s10404-012-0999-2].

[41] E. M. Fenton, M. R. Mascarenas, G. P. López, and S. S. Sibbett, "Multiplex lateral-flow test strips fabricated by two-dimensional shaping.," *ACS applied materials & interfaces* **1**(1), 124–129 (2009) [doi:10.1021/am800043z].

[42] A. W. Martinez, S. T. Phillips, M. J. Butte, and G. M. Whitesides, "Patterned paper as a platform for inexpensive, low-volume, portable bioassays.," *Angewandte Chemie (International ed. in English)* **46**(8), 1318–1320 (2007) [doi:10.1002/anie.200603817].

[43]   A. W. Martinez, S. T. Phillips, and G. M. Whitesides, "Three-dimensional microfluidic devices fabricated in layered paper and tape.," *Proceedings of the National Academy of Sciences of the United States of America* **105**(50), 19606–19611 (2008) [doi:10.1073/pnas.0810903105].

[44]   H. Noh and S. T. Phillips, "Fluidic timers for time-dependent, point-of-care assays on paper.," *Analytical chemistry* **82**(19), 8071–8078 (2010) [doi:10.1021/ac1005537].

[45]   H. Noh and S. T. Phillips, "Metering the capillary-driven flow of fluids in paper-based microfluidic devices.," *Analytical chemistry* **82**(10), 4181–4187 (2010) [doi:10.1021/ac100431y].

[46]   G. E. Fridley, H. Q. Le, E. Fu, and P. Yager, "Controlled release of dry reagents in porous media for tunable temporal and spatial distribution upon rehydration.," *Lab on a chip* **12**(21), 4321–4327 (2012) [doi:10.1039/c2lc40785j].

[47]   E. Fu, "Chemical signal amplification in two-dimensional paper networks," 325–328 (2011) [doi:10.1016/j.snb.2010.06.024.Chemical].

[48]   E. Fu, T. Liang, P. Spicar-Mihalic, J. Houghtaling, S. Ramachandran, and P. Yager, "Two-dimensional paper network format that enables simple multistep assays for use in low-resource settings in the context of malaria antigen detection.," *Analytical chemistry* **84**(10), 4574–4579 (2012) [doi:10.1021/ac300689s].

[49]   E. Fu, B. Lutz, P. Kauffman, and P. Yager, "Controlled reagent transport in disposable 2D paper networks.," *Lab on a chip* **10**(7), 918–920 (2010) [doi:10.1039/b919614e].

[50]   E. Fu, S. a. Ramsey, P. Kauffman, B. Lutz, and P. Yager, "Transport in two-dimensional paper networks," *Microfluidics and Nanofluidics* **10**(1), 29–35 (2010) [doi:10.1007/s10404-010-0643-y].

[51] B. R. Lutz, P. Trinh, C. Ball, E. Fu, and P. Yager, "Two-dimensional paper networks: programmable fluidic disconnects for multi-step processes in shaped paper.," *Lab on a chip* **11**(24), 4274–4278 (2011) [doi:10.1039/c1lc20758j].

[52] J. L. Osborn, B. Lutz, E. Fu, P. Kauffman, D. Y. Stevens, and P. Yager, "Microfluidics without pumps: reinventing the T-sensor and H-filter in paper networks.," *Lab on a chip* **10**(20), 2659–2665 (2010) [doi:10.1039/c004821f].

[53] E. Fu, T. Liang, J. Houghtaling, S. Ramachandran, S. A. Ramsey, and B. Lutz, "Enhanced sensitivity of lateral flow tests using a two-dimensional paper network format," 7941–7946 (2011).

[54] E. Fu, P. Kauffman, B. Lutz, and P. Yager, "Chemical signal amplification in two-dimensional paper networks.," *Sensors and actuators. B, Chemical* **149**(1), 325–328, Elsevier B.V. (2010) [doi:10.1016/j.snb.2010.06.024].

[55] E. Fu, T. Liang, P. Spicar-Mihalic, J. Houghtaling, S. Ramachandran, and P. Yager, "Two-dimensional paper network format that enables simple multistep assays for use in low-resource settings in the context of malaria antigen detection.," *Analytical chemistry* **84**(10), 4574–4579 (2012) [doi:10.1021/ac300689s].

[56] D. Ns and D. K. Nordborg, "Microfluidics - a review" (1993).

[57] a. N. Chatterjee and N. R. Aluru, "Combined circuit/device modeling and simulation of integrated microfluidic systems," *Journal of Microelectromechanical Systems* **14**(1), 81–95 (2005) [doi:10.1109/JMEMS.2004.839025].

[58] C. J. C. Biscombe, M. R. Davidson, and D. J. E. Harvie, "membranes," *Colloids and Surfaces A: Physicochemical and Engineering Aspects*, Elsevier B.V. (2012) [doi:10.1016/j.colsurfa.2012.10.037].

[59] A. Rasmussen, C. Mavriplis, M. E. Zaghloul, O. Mikulchenko, and K. Mayaram, "Simulation and optimization of a micro ‾uidic ‾ow sensor" (2001).

[60] Y. Zhao, D. Chen, Y. Luo, H. Li, B. Deng, S.-B. Huang, T.-K. Chiu, M.-H. Wu, R. Long, et al., "A microfluidic system for cell type classification based on cellular size-independent electrical properties.," *Lab on a chip* **1**(c), 2272–2277 (2013) [doi:10.1039/c3lc41361f].

[61] J.-L. Hong, K.-C. Lan, and L.-S. Jang, "Electrical characteristics analysis of various cancer cells using a microfluidic device based on single-cell impedance measurement," *Sensors and Actuators B: Chemical* **173**, 927–934, Elsevier B.V. (2012) [doi:10.1016/j.snb.2012.06.046].

[62] L. Kim, M. D. Vahey, H.-Y. Lee, and J. Voldman, "Microfluidic arrays for logarithmically perfused embryonic stem cell culture.," *Lab on a chip* **6**(3), 394–406 (2006) [doi:10.1039/b511718f].

[63] W. M. Weaver, S. Dharmaraja, V. Milisavljevic, and D. Di Carlo, "The effects of shear stress on isolated receptor-ligand interactions of Staphylococcus epidermidis and human plasma fibrinogen using molecularly patterned microfluidics.," *Lab on a chip* **11**(5), 883–889 (2011) [doi:10.1039/c0lc00414f].

[64] W. M. Weaver, V. Milisavljevic, J. F. Miller, and D. Di Carlo, "Fluid flow induces biofilm formation in Staphylococcus epidermidis polysaccharide intracellular adhesin-positive clinical isolates.," *Applied and environmental microbiology* **78**(16), 5890–5896 (2012) [doi:10.1128/AEM.01139-12].

[65] A. Ajdari, "Steady flows in networks of microfluidic channels: building on the analogy with electrical circuits," *Comptes Rendus Physique* **5**(5), 539–546 (2004) [doi:10.1016/j.crhy.2004.02.012].

[66] T. Bourouina and J.-P. Grandchamp, "Modeling micropumps with electrical equivalent networks," *Journal of Micromechanics and Microengineering* **6**(4), 398–404 (1996) [doi:10.1088/0960-1317/6/4/006].

[67] S. Mendez, E. M. Fenton, G. R. Gallegos, D. N. Petsev, S. S. Sibbett, H. a Stone, Y. Zhang, and G. P. López, "Imbibition in porous membranes of complex shape: quasi-stationary flow in thin rectangular segments.," *Langmuir : the ACS journal of surfaces and colloids* **26**(2), 1380–1385 (2010) [doi:10.1021/la902470b].

[68] J. R. Buser, G. Kimpel, P. Kauffman, E. Fu, B. Lutz, and P. Yager, "Centrifugal force-based characterization of membranes used in paper microfluidics," 4574 (2012).

[69] E. W. Washburn, "The Dynamics of Capillary Flow," *Phys. Rev* **17**(3), 273 (1921).

[70] R. Lucas, "Ueber das Zeitgesetz des Kapillaren Aufstiegs von Fullisgkeiten," *Kolloid Z.* **23**(15) (1918).

[71] World Health Organization, "WHO | Data and statistics," World Health Organization.

[72] PATH, "Preventing HIV/AIDS in Low-Resource Settings," *Outlook* **19**(1), 1–9 (2001).

[73] R. O. Valdiserri, D. R. Holtgrave, and G. R. West, "Promoting early HIV diagnosis and entry into care.," *AIDS (London, England)* **13**(17), 2317–2330 (1999).

[74] C. D. Pilcher, H. C. Tien, J. J. Eron, P. L. Vernazza, S.-Y. Leu, P. W. Stewart, L.-E. Goh, and M. S. Cohen, "Brief but efficient: acute HIV infection and the sexual transmission of HIV.," *The Journal of infectious diseases* **189**(10), 1785–1792 (2004) [doi:10.1086/386333].

[75] E. H. I. V Incidence, D. Acute, and H. I. V Infection, "Assays to Estimate HIV Incidence and Detect Acute HIV Infection Global Landscape & Market Assessments," *Health (San Francisco).*

[76] A. Nabatiyan, M. a Baumann, Z. Parpia, and D. Kelso, "A lateral flow-based ultra-sensitive p24 HIV assay utilizing fluorescent microparticles.," *Journal of acquired immune deficiency syndromes (1999)* **53**(1), 55–61 (2010) [doi:10.1097/QAI.0b013e3181c4b9d5].

[77]   A. J. De Baets, B. S. Edidi, M. J. Kasali, G. Beelaert, W. Schrooten, A. Litzroth, P. Kolsteren, D. Denolf, and K. Fransen, "Pediatric Human Immunodeficiency Virus Screening in an African District Hospital," *Society* **12**(1), 86–92 (2005) [doi:10.1128/CDLI.12.1.86].

[78]   WHO, "Global HIV/AIDS Response: Epidemic update and health sector progress towards Universal Access" (2011).

[79]   P. Patel, B. Bennett, T. Sullivan, M. M. Parker, J. D. Heffelfinger, and P. S. Sullivan, "Rapid HIV screening: missed opportunities for HIV diagnosis and prevention.," in *Journal of clinical virology : the official publication of the Pan American Society for Clinical Virology* **54**(1), pp. 42–47 (2012) [doi:10.1016/j.jcv.2012.01.022].

[80]   BioRad, "Combo Ag/Ab EIA."

[81]   A. Zolopa, J. Andersen, W. Powderly, A. Sanchez, I. Sanne, C. Suckow, E. Hogg, and L. Komarow, "Early antiretroviral therapy reduces AIDS progression/death in individuals with acute opportunistic infections: a multicenter randomized strategy trial.," *PloS one* **4**(5), e5575 (2009) [doi:10.1371/journal.pone.0005575].

[82]   P. Clayden, "High rates of HIV acquisition in pregnancy and post partum in Francistown, Botswana" (2009).

[83]   S. L. Stramer, S. a Glynn, S. H. Kleinman, D. M. Strong, S. Caglioti, D. J. Wright, R. Y. Dodd, and M. P. Busch, "Detection of HIV-1 and HCV infections among antibody-negative blood donors by nucleic acid-amplification testing.," *The New England journal of medicine* **351**(8), 760–768 (2004) [doi:10.1056/NEJMoa040085].

[84]   E. W. Fiebig, D. J. Wright, B. D. Rawal, P. E. Garrett, R. T. Schumacher, L. Peddada, C. Heldebrant, R. Smith, A. Conrad, et al., "Dynamics of HIV viremia and antibody seroconversion in plasma donors: implications for diagnosis and staging of primary HIV infection.," *AIDS (London, England)* **17**(13), 1871–1879 (2003) [doi:10.1097/01.aids.0000076308.76477.b8].

[85] G. a Posthuma-Trumpie, J. Korf, and A. van Amerongen, "Lateral flow (immuno)assay: its strengths, weaknesses, opportunities and threats. A literature survey.," *Analytical and bioanalytical chemistry* **393**(2), 569–582 (2009) [doi:10.1007/s00216-008-2287-2].

[86] R. Coombs, "Laboratory diagnosis of HIV infection revisited," in *Point-of-Care Daignostics for Global Health* (2012).

[87] M. N. SASI group, "HIV Prevalence," 2004, <www.worldmapper.com>.

APPENDIX I

In MATLAB, we used the 'polyfit' command to determine the slope of the line that resulted from plotting fluid migration data in the form of time versus length squared. The slopes from three different trials were averaged; C_{LW} was determined to be 11.6 mm²/sec ± 0.2 mm²/sec (n=3). All relevant data for this calculation is shown below (**Figure 24,**

Table *7*). MATLAB's 'regstats' command was used to determine R^2 values for each trial.
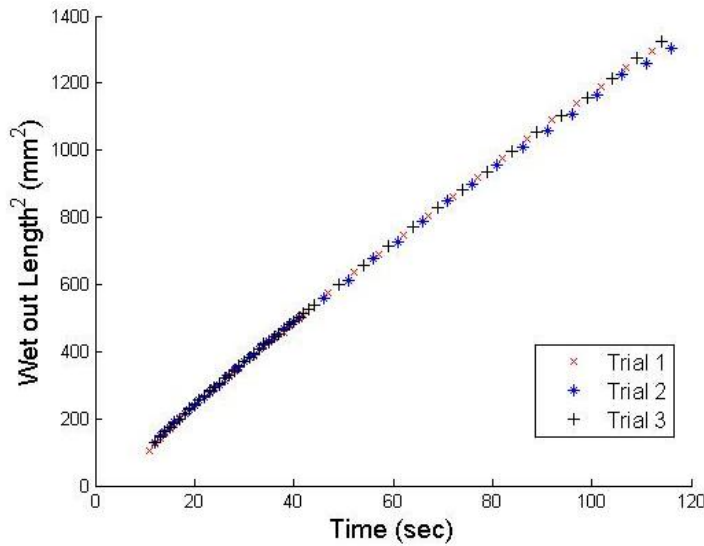
Figure 24. Experimental determination of the Lucas-Washburn coefficient. The slope of the line generated by plotting wet out time versus the square of fluid wet out length (from an ideal well source) corresponds to the previously defined C_{LW} constant. This value holds true for an HF135 nitrocellulose wicking membrane and colored dye (diluted in water) solution. Data points from all three experimental trials are shown.

Table 7. *Determination of Lucas-Washburn Coefficient, C_{LW}.*

	Slope (C_{LW}) [mm²/sec]	R^2
Trial 1	11.8	0.9987
Trial 2	11.4	0.9984
Trial 3	11.6	0.9991
Average	**11.6 ± 0.2**	

MATLAB Code:

```matlab
figure
hold on
num4=xlsread('Washburn.xlsx'); %Read in Excel data

%Trial 1
plot(num4(1:46,1),num4(1:46,2),'rx')
P1=polyfit(num4(1:46,1),num4(1:46,2),1); %Determine slope of plot
stats1 = regstats(num4(1:46,1),num4(1:46,2),'linear','rsquare');
%Determine R2 value

%Trial 2
plot(num4(1:45,5),num4(1:45,6),'b*')
P2=polyfit(num4(1:45,5),num4(1:45,6),1);
stats2 = regstats(num4(1:45,5),num4(1:45,6),'linear','rsquare');

%Trial 3
plot(num4(:,7),num4(:,8),'k+')
P3=polyfit(num4(:,7),num4(:,8),1);
stats3 = regstats(num4(:,7),num4(:,8),'linear','rsquare');

%Calculate average Lucas-Washburn coefficient value
CLW_all=[P1(1),P2(1),P3(1)];
CLW=mean(CLW_all);
CLWsd=std(CLW_all);

%Set plot style
h_legend=legend('Trial 1','Trial 2','Trial 3');
set(h_legend,'FontSize',12);
xlabel('Time (sec)','FontSize',14)
ylabel('Wet out Length^2 (mm^2)','FontSize',14)
hold off
```

APPENDIX II

The analytical equations for the rate of fluid release from the three sources in the Pseudo-1DPN were derived using the circuit model shown in **Figure 13** (**Table 8**).

Table 8. Analytical system model for a Pseudo-1DPN with three fluid sources.

	Source 1	Source 2	Source 3
Stage One	$Q_1 = \dfrac{P_P - P_S(1)}{R(t)}$	$Q_2 = \dfrac{P_s(1) - P_S(2)}{R_S(1)}$	$Q_3 = \dfrac{P_s(2) - P_S(3)}{R_S(2)}$
Stage Two	-	$Q_2 = \dfrac{P_P - P_S(2)}{R_S(1) + R(t)}$	$Q_3 = \dfrac{P_s(2) - P_S(3)}{R_S(2)}$
Stage Three	-	-	$Q_3 = \dfrac{P_P - P_S(3)}{R_S(2) + R_S(1) + R(t)}$

APPENDIX III

Table 9. Overview of system parameters and variables used in the computational model.

	Variable	Definition	Method of Determination	Value	Units
Wicking membrane	P_P	Capillary pressure of the wicking membrane	Experimentally	1.08×10^4	Pa
	κ	Membrane permeability	Experimentally	5.5×10^{-13}	m^2
	H	Membrane thickness	Material specification	1.35×10^{-4}	m
	W	Strip width	Tunable design parameter	-	m
	Cap	Fluidic capacity (volume/area)	Experimentally	9.24×10^{-5}	m
	L_S	Length of wicking membrane between two sources	Tunable design parameter	-	m
	L_{over}	Length of membrane succeeding final source	Tunable design parameter	-	m
	L_0	Length of membrane wet out after initial fluid release (initial condition)	Generated by computational model	-	m
Fluid Sources	P_S	Backpressure exerted by a given source	Experimentally, design parameter	-	Pa
	V_{Tot}	Initial volume supplied to a given source	Tunable design parameter	-	m^3
	V	Volume retained by a given source	Generated by computational model	-	m^3
	α	Fraction of volume retained by a given source	Generated by computational model	-	-
	Q	Volumetric flow rate of a given fluid through the membrane	Generated by computational model	-	m^3/s
	L_P	Length of a given source	Tunable design parameter	-	m
	μ	Fluid viscosity	Literature value	10^{-3}	kg/m·s

APPENDIX IV

Implementation of the computational model was divided into three key sections: define relevant system parameters, define initial conditions, and track system progress over time. We provide a detail description of each section in this appendix.

Define relevant system parameters. This includes inherent properties of the wicking membrane and fluids (P_P, κ, H, cap, μ), as well as device design parameters (W, V_{Tot}, L_S, L_{over}, L_P). Properties of the wicking membrane were determined experimentally (P_P, cap, κ) or using material specifications (H). HF135 nitrocellulose capillary pressure and permeability were determined by Joshua Buser and George Kimpel from the Yager Lab [68]. Device design parameters were initially chosen in consideration of previously demonstrated 2DPN devices; these parameters can be easily altered to fit the system of interest.

Define initial conditions. We considered system behavior only after initial wet out occurred; some amount of fluid was already released from the sources and sections of the membrane were either partially or fully wetted. We assumed fluid from two neighboring sources met midway between their spacer region. This region of membrane was fully wetted, corresponding to a constant R_S value. The membrane region to the right of S_1 (R(t)) was partially wetted; the fluid front progressed the same distance to the right and left of the source during initial wet-out. As a note, for initial wet-out from all sources to terminate at the same time, the fluids must travel

equivalent distances; spacing between all sources ($L_S(1)$,$L_S(2)$) must be equal for the purpose of this model.

The length of wet-out associated with each source (L_0) was defined as:

$$L_0(1) = 0.5L_S(1) + L_P(1) + 0.5L_S(1) \tag{23}$$

$$L_0(2) = 0.5L_S(2) + L_P(2) + 0.5L_S(1) \tag{24}$$

$$L_0(3) = L_{over} + L_P(3) + 0.5L_S(2) \tag{25}$$

These distance were converted to volume released using the membrane's capacity and width. Fluidic resistances for each membrane region [($R_S(1)$, $R_S(2)$, $R(t)$] were calculated using Equation 1 ($R=\mu L/\kappa WH$). Wet out lengths associated with the resistances (L) referred to either spacer distances or the fluid column length to the right of S_1; the region of wicking membrane underneath each source was not included in these resistance calculations.

We calculated the initial volumetric flow rate of each source fluid through the membrane using the Stage One equations defined in **Table 8** . All necessary resistance values were determined above and the backpressure associated with each source was either a known, constant value or could be calculated based on source saturation values.

In summary, in this section of the model, we determined the following initial conditions after initial wet-out: length of membrane wet-out (L), volume released from each source (V), percentage of fluid retained by each source (α), resistance of relevant membrane regions [R_s, $R(t)$], source backpressure (P_S), and initial flow rate of each source reagent (Q). This set of

variables was calculated at each point in time in the subsequent section to describe the system's behavior.

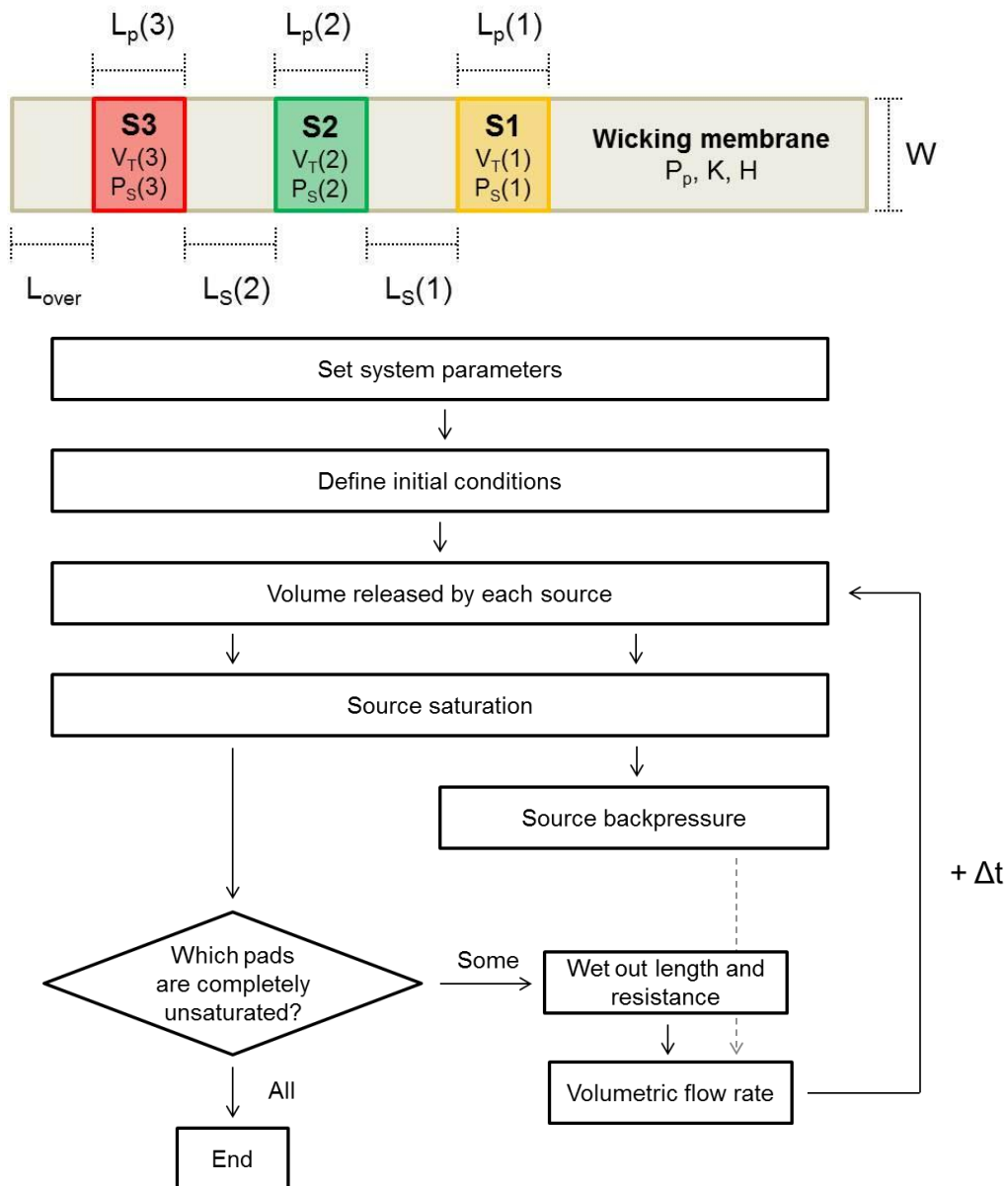**Track system progress over time.** Using a 'for' loop and the previously determined initial

Figure 13. Computational model design for a Pseudo-1DPN with three delivery steps. A) Schematic of modeled device with critical system parameters labeled. B) Flow chart that outlines the overall implementation process for determining the fluidic behavior of the Pseudo-1DPN in MATLAB.

conditions, we tracked critical variables within the system over time. We chose a time-step (t_{step}) of 1 second. For each point in time, we calculate the same set of variables determined in the previous section (V, α, R_S, $R(t)$, P_S, Q). For a given time j, we determine the updated volume of fluid released from each source by considering the flow rate at time j - 1. For example, for the first source,

$$V_1(j) = V_1(j-1) + Q_1(j-1) * t_{step} \tag{26}$$

This volume was compared to the total volume of each source (V_{Tot}) to determine source saturation (α). If the backpressure exerted by each source was a function of its saturation, this saturation value was used to determine source backpressure. Additionally, based on the sign of α, we determined what stage of delivery we are operating. For example, if the saturation of the first source was less than or equal to zero ($\alpha(1) \leq 0$) but the other two source still retained some fluid, we assumed we were in Stage Two of the device; the first source had been completely depleted.

We also used the amount of volume released from the sources to measure the progression of the fluid front through the membrane. For Sources 2 and 3 during Stage One, it was unnecessary to take these volume affects into account as the length of the spacer region, and consequentially, its associated resistance, was constant. However, the resistance $R(t)$ increased as more fluid was released into the membrane from Source 1. In this case, we simply increased the fluid wet-out length associated with $R(t)$ to reflect the additional amount of volume released from the source over the time interval.

As a note, we can imagine that leakage flow from Sources 2 and 3 had additional effects on this wet-out length, as it pushed fluid past the spacer regions, into the rightmost region of the membrane. However, we ignored these effects in this first generation model due to a limited knowledge of how fluid behaved once reaching a partially saturated source. It was unknown whether the fluid preferentially traveled into and through the source, underneath the source through the membrane, or a combination of both. For example, we had seen that if a fluid front came into contact with a partially saturated glass fiber pads, some of the fluid was taken up in the pad. However, if that pad was completely dry or unsaturated, the fluid front progressed underneath the pad, through the nitrocellulose wicking membrane. These preliminary experiments suggested that, similar to fluid release from a source, the path of a fluid front into a source is largely determined by the saturation of the pad – a complexity that we were unable to account for in this model.

In Stage Two of operation, only the spacer resistance between the second and third sources remained constant. The resistance associated with the membrane region to the right of Source 2 increased as additional fluid was released from the source. We redefined this resistance to include length contributions from the spacer region between Sources 1 and 2 $[L_S(1)]$, the width of Source 1 $[L_P(1)]$, and the wet out length associated with the previous stage of fluid release. We tracked the additional volume of fluid released by the second source from the initiation of Stage Two and include its impact on wet-out length and membrane resistance. Wet-out resistance in Stage Three of delivery was defined similarly.

Once the resistance of each membrane region was calculated, we determined the volumetric release rate from each source. The equation used for a given source depended on the stage of delivery. We used these flow rates to re-enter the loop and consider behavior at the next point in time ($j + 1$). This loop continued until all sources were completely unsaturated.

APPENDIX V

```
%% PSEUDO-1DPN DEVICE WITH CAPILLARY TUBE SOURCES

%% Set parameters and variables
Vtot=10^-8*[1.5 1.5 1.5];
Tstep=1;
PP=10800;
u=0.001;
w=0.004;
h=1.35*10^(-4);
k=0.55*10^-12;
Lover=0.002125;
Ls=[.00425 .00425];
Lp=[0.002 0.002 0.002];
Cap=w*11.3*10^-5; %[volume/length traveled]

%% Set initial conditions
r12=(u*Ls(1))/(k*w*h); %Resistance of spacer segment [kg/m^4*s]
r23=(u*Ls(2))/(k*w*h);
%Initial position of the fluid front assuming that it wets out
%to half way position
L0=[Lp(1)+0.5*Ls(1)+0.5*Ls(1) Lp(2)+0.5*Ls(2)+0.5*Ls(1)
Lp(3)+Lover+0.5*Ls(2)];
L=zeros(1,100000); %Fluid front progression from Source 1
L(1)=0.5*Ls(1);
L1=zeros(1,100000); %Fluid front progression from Sources 2,3
R=zeros(1,100000); %Time dependent resistance associated with Source 1
R(1)=(u*L(1))/(k*w*h);
R1=zeros(1,100000);
Ldrain=zeros(3,100000); %Length traveled by the fluid due to leakage
flow
Vdrain=zeros(3,100000); %Additional volume drained after the previous
pad is drained

%Initial condition for drained volume
V=zeros(3,100000);
V(1,1)=L0(1)*Cap;
V(2,1)=L0(2)*Cap;
V(3,1)=L0(3)*Cap;

%Initial condition for pad percent saturation
alpha=zeros(3,100000);
alpha(1,1)=(Vtot(1)-V(1,1))/Vtot(1);
alpha(2,1)=(Vtot(2)-V(2,1))/Vtot(2);
alpha(3,1)=(Vtot(3)-V(3,1))/Vtot(3);

%Initial condition for pad pressures
PS=zeros(3,100000);
```

```matlab
grav=9.8;
dens=1000;
rad=Lp/2;
Pcap=154;

Pgrav=zeros(3,100000);
Pgrav(1,1)=dens*grav*(Vtot(1)-V(1,1))/(pi*rad(1)^2);
Pgrav(2,1)=dens*grav*(Vtot(2)-V(2,1))/(pi*rad(2)^2);
Pgrav(3,1)=dens*grav*(Vtot(3)-V(3,1))/(pi*rad(3)^2);

PS(1,1)=Pcap-Pgrav(1,1);
PS(2,1)=Pcap-Pgrav(2,1);
PS(3,1)=Pcap-Pgrav(3,1);

%Initial condition for flow rate
Q=zeros(3,100000);
Q(1,1)=(-1*PS(1,1)+PP)/R(1);
Q(2,1)=(-1*PS(2,1)+PS(1,1))/r12;
Q(3,1)=(-1*PS(3,1)+PS(2,1))/r23;

%% Track movement of the fluids in time

for j=2:100000

    %Adjust depletion volume based on previous flow rate
    V(1,j)=V(1,j-1)+Q(1,j-1)*Tstep;
    V(2,j)=V(2,j-1)+Q(2,j-1)*Tstep;
    V(3,j)=V(3,j-1)+Q(3,j-1)*Tstep;

    %Ensures non-negative saturation values
    if V(1,j)>=Vtot(1)
        V(1,j)=Vtot(1);
    end
    if V(2,j)>=Vtot(2)
        V(2,j)=Vtot(2);
    end
    if V(3,j)>=Vtot(3)
        V(3,j)=Vtot(3);
    end

    alpha(1,j)=(Vtot(1)-V(1,j))/Vtot(1);
    alpha(2,j)=(Vtot(2)-V(2,j))/Vtot(2);
    alpha(3,j)=(Vtot(3)-V(3,j))/Vtot(3);

    Pgrav(1,j)=dens*grav*(Vtot(1)-V(1,j))/(pi*rad(1)^2);
    Pgrav(2,j)=dens*grav*(Vtot(2)-V(2,j))/(pi*rad(2)^2);
    Pgrav(3,j)=dens*grav*(Vtot(3)-V(3,j))/(pi*rad(3)^2);

    PS(1,j)=Pcap-Pgrav(1,j);
    PS(2,j)=Pcap-Pgrav(2,j);
```

```matlab
        PS(3,j)=Pcap-Pgrav(3,j);

    % Case where all the pads are still draining
    if (alpha(1,j)>0 && alpha(2,j)>0 && alpha(3,j)>0)

        L(j)=(V(1,j)/Cap)-L0(1)+L(1);
        R(j)=(u*L(j))/(k*w*h);

        Q(1,j)=(-1*PS(1,j)+PP)/R(j);
        Q(2,j)=(-1*PS(2,j)+PS(1,j))/r12;
        Q(3,j)=(-1*PS(3,j)+PS(2,j))/r23;

        Lend=L(j); %Distance of the fluid from Source 1 in the NC
        v2end=V(2,j); %Volume drained from Source 2 when Source 1 is
drained

        % Case where the first sourcce is completely drained
    elseif (alpha(2,j)>0 && alpha(3,j)>0 && alpha(1,j)<=0)

        Vdrain(2,j)=V(2,j)-v2end;
        Ldrain(2,j)=Vdrain(2,j)/Cap; %Length of fluid released from
Source 2 since Source 1 has drained
        L1(j)=Ls(1)+Lp(1)+Lend+Ldrain(2,j); %New wet out length
        R1(j)=(u*L1(j))/(k*w*h);

        Q(1,j)=(-1*PS(2,j)+PP)/R1(j);
        Q(2,j)=(-1*PS(2,j)+PP)/R1(j);
        Q(3,j)=(-1*PS(3,j)+PS(2,j))/r23;

        L2end=L1(j); %Distance of fluid from Source 2 in the NC
        v3end=V(3,j); %volume drained from Source 3 when Source 2 is
drained

        % Case where first two sources are completely drained
    elseif (alpha(3,j)>0 && alpha(2,j)<=0 && alpha(1,j)<=0)

        Vdrain(3,j)=V(3,j)-v3end;
        Ldrain(3,j)=Vdrain(3,j)/Cap;
        L1(j)=Ls(2)+Lp(2)+L2end+Ldrain(3,j);
        R1(j)=(u*L1(j))/(k*w*h);

        Q(1,j)=(-1*PS(3,j)+PP)/R1(j);
        Q(2,j)=(-1*PS(3,j)+PP)/R1(j);
        Q(3,j)=(-1*PS(3,j)+PP)/R1(j);

    else
        break
    end
end
```

98

APPENDIX VI

Capillary pressure is a function of surface tension (γ), interface radius (r), and contact angle (θ):

$$P_{cap} = \frac{2\gamma \cos\theta}{r} \tag{27}$$

Capillary pressure is constant for a given tube size, fluid, and contact material; the capillary pressure of all sources in our device should be equivalent. Gravitational pressure is a function of the gravitational acceleration of the Earth (*g*), the density of the fluid (ρ), and the height of the fluid column in the tube (h):

$$P_{grav} = \rho gh \tag{28}$$

The gravitational pressure of fluid in a vertical tube will decrease as fluid is released. Thus, the backpressure exerted by a capillary tube theoretically varies with source depletion.

The capillary pressure of a 2mm diameter tube (containing water) was determined to be 0.154 ± 0.002 kPa (n=3) (**Table 10**). This value was determined by placing the capillary in a large fluid source and measuring the height of fluid retained by the capillary once removed from the source. The capillary and gravitational pressures were equally balanced at this fluid height. Thus, the capillary pressure of the tube could be calculated using Equation 28.

The gravitational pressure exerted by fluid in a capillary depends on the volume contained. We used a maximum of 15 µL H_2O per capillary in our system, which corresponds to a pressure of approximately 0.047 kPa. This was calculated by rewriting Equation 28 as a function of fluid volume and tube radius (rather than fluid height):

$$P_{grav} = \rho g \left(\frac{V}{\pi R^2}\right) \qquad (29)$$

The total backpressure exerted a given capillary in this set-up ranges from 0.107 kPa to 0.153 kPa, which is insignificant in comparison to the capillary pressure of an HF135 nitrocellulose wicking membrane (<0.015% of 10.8 kPa). The volume-dependent pressure effects of capillary tubes should have little effect on device behavior, in comparison to that achieved using perfect, ideal sources.

Table 10. Experimental determination of the capillary pressure exerted by a 2 mm diameter capillary tube.

	Maximum Fluid Height [mm]	Capillary Pressure (Pa)
Trial 1	15.7	154
Trial 2	15.4	151
Trial 3	15.9	156
Average	11.7 ± 0.2	154 ± 2

APPENDIX VII

Four possible sources of error in the computational model include:

- The incorporation of inaccurate system parameter values into the model

- The model's inability to account for all consequences of leakage flow

- Optical aberrations from the web camera

- Flow abnormalities from contact between capillary tubes and the wicking membrane

Membrane parameters, such as capillary pressure, permeability, and capacity, are difficult to quantify due to the complex, non-uniform structure of the porous medium. These parameters are not provided by the manufacturing company and consequentially had to be experimentally determined for model use. Membrane characteristics may also vary between material batches, and thus, an accurate description of one membrane may not hold true for an alternative sheet of the same material.

In the model, we ignored any effects of leakage flow on downstream flow and resistance values, assuming their effects are negligible. This does not capture total device behavior and may prove to be a critical factor to consider.

Experimentally, we found there to be a clear discrepancy between wet out length and the calculated volume delivered. Using wet out length to measure volume released showed Sources 2 and 3 never completely delivered their fluidic load; they both released only ~93% of their original contents. However, visual observation of the fluid remaining in the capillary showed completely

delivery was actually achieved. This deviation may be attributed to an inaccurate membrane capacity value, but could also be partially caused by optical aberrations from the web camera. The long length of the wicking membrane might have caused image scaling to vary based on camera location and the point of interest. We attempted to account for this potential error by using ruler markings near the strip to scale the image as a function of position. However, this might not have been sufficient to remove all aberrations caused by the camera.

Finally, it is possible that contact between capillary tubes and the nitrocellulose membrane caused flow abnormalities. To ensure all tubes remained in contact with the membrane, force was applied to push the capillaries onto the membrane. This might have damaged the membrane structure and resulted in unpredicted flow behaviors. This non-ideality could be removed by designing an alternate method for establishing contact between capillaries and the membrane (*i.e.,* use an intermediate between tube and membrane to deliver fluid from the sources).

APPENDIX VIII
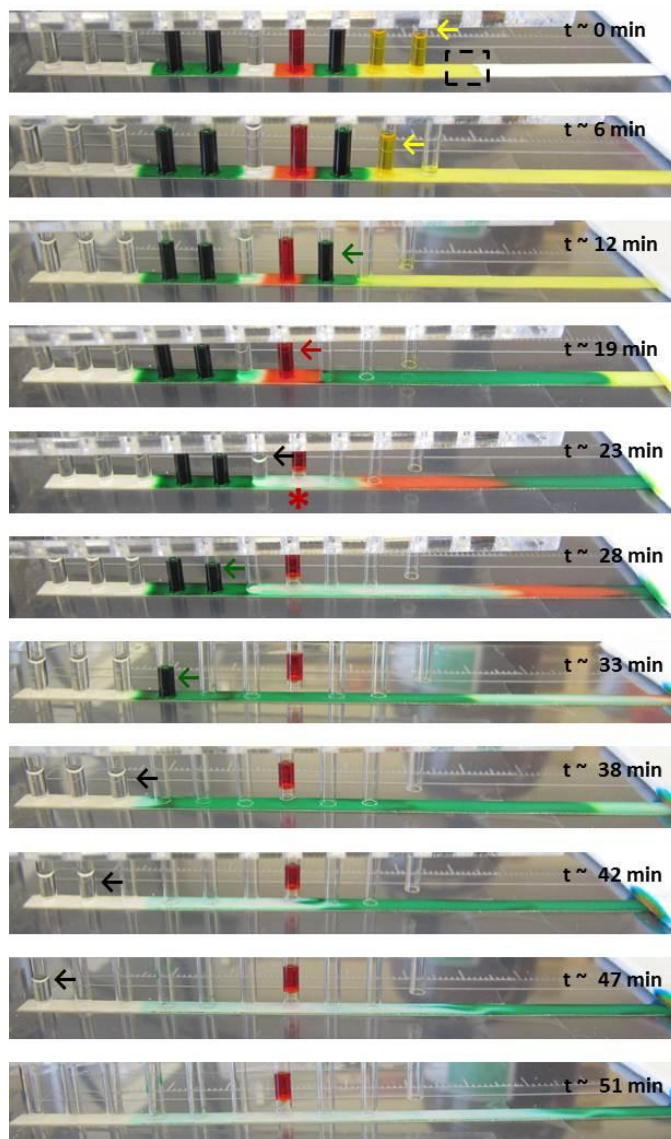
Figure 25. Sequential delivery in a Pseudo-1DPN with ten capillary tube sources. Each color represented a specific reagent delivery step in the p24 antigen assay (yellow: sample; red: biotin-antibody; green(1): streptavidin-HRP; green(2,3): DAB). Water without food coloring (clear) represented PBST wash steps. Sequential delivery was achieved for all reagents. There was little mixing between source fluids and the fluid front interface between reagents was distinct. Red fluid was not delivered in its entirety because the capillary lost contact with the membrane midway through delivery (marked by *); this highlighted the importance of maintaining contact between all capillaries and the wicking membrane. All green fluid/DAB was pushed through the theoretical capture area (dashed rectangle to the right of the first source) by the three PBST washes. Arrows are used to denote the current stage of operation.